

A solvable model for strongly interacting nonequilibrium excitons

Zhenhao Song,^{1,*} Tessa Cookmeyer,^{2,*} and Leon Balents^{2,3,4}

¹*Physics Department, University of California, Santa Barbara, California 93106-4030, USA*

²*Kavli Institute for Theoretical Physics, University of California, Santa Barbara, California 93106-4030, USA*

³*Canadian Institute for Advanced Research, Toronto, Ontario, Canada*

⁴*French American Center for Theoretical Science, CNRS, KITP, Santa Barbara, California 93106-4030, USA*

We study the driven-dissipative Bose-Hubbard model with all-to-all hopping and subject to incoherent pumping and decay, as is naturally probed in several recent experiments on excitons in WS₂/WSe₂ moiré systems, as well as quantum simulators. By positing a particular form of coupling to the environment, we derive the Lindblad jump operators and show that, in certain limits, the system admits a closed-form expression for the steady-state density matrix. Away from the exactly solvable regions, the steady-state can be obtained numerically for 100s-1000s of sites. We study the nonequilibrium phase diagram and phase transitions, which qualitatively matches the equilibrium phase diagram, agreeing with the intuition that increasing the intensity of the light is equivalent to changing the bosonic chemical potential. However, the steady-states are far from thermal states and the nature of the phase transitions is changed.

I. INTRODUCTION

The Bose-Hubbard model is the paradigmatic model of interacting bosons on a lattice and describes a transition between a Mott insulating and superfluid phase [1]. There are now several platforms for experimentally realizing this model such as trapped bosonic atoms [2–6] or photon modes [7–9]. In the latter case, interactions are induced through circuit quantum electrodynamics (QED) [10, 11], cavity QED [12–15], semiconductor platforms [16–18], or Rydberg atoms [19, 20], and a lattice can be produced by interconnecting these platforms [15, 18, 21]. Excitons in transition-metal dichalcogenide moiré bilayers [22–24] or artificial lattices [25] provide another emerging solid-state realization of Bose-Hubbard physics, where the interactions are naturally implemented through strong dipole repulsions. All these experimental settings move beyond the study of equilibrium physics as these systems either controllably couple to their environments or have finite lifetimes for the bosons [10, 26].

We are most interested in understanding several recent experiments potentially realizing bosonic Mott physics with excitons in WSe₂/WS₂ moiré bilayers [27–31]. The experiments see a finite energy shift in photoluminescence spectrum interpreted as an on-site exciton-exciton interaction with multiple excitons per site. There is considerable evidence that the excitons enter an interaction-dominated Mott-insulating regime at sufficiently large intensities of light [27, 30]. The inherently non-equilibrium nature of these experiments, given the necessity of continuously pumping the system full of decaying excitons, naturally raise the question of how much these reported nonequilibrium Mott phases resemble their equilibrium counterpart, and whether an analog of the superfluid phase exists out of equilibrium.

The Bose-Hubbard model,

$$H_0 = \mu \sum_i n_i + \frac{U}{2} \sum_i n_i(n_i - 1) - \sum_{i,j} t_{i,j} b_i^\dagger b_j, \quad (1)$$

subject to dissipation and driving, is the prototypical model for studying strongly interacting open quantum systems. The drive is often coherently added to the total Hamiltonian, $H_{\text{tot}} = H_0 + F b_i^\dagger + F^* b_i$, and the decay is implemented through a Lindblad master equation for the density matrix ρ [32–34],

$$\dot{\rho} = -i[H_0, \rho] + \sum_{k,k'} \gamma_{k,k'} \mathcal{L}(L_k, L_{k'}^\dagger)[\rho] \quad (2)$$

where $\mathcal{L}(A, B)[\rho(t)] = A\rho(t)B - \frac{1}{2}\{BA, \rho(t)\}$, L_k are the jump operators and $\gamma_{k,k'}$ are the associated damping rates. By including suitable Lindblad jump operators, we can include incoherent driving as the reverse process of decay.

This system has been numerically studied with numerous methods: mean-field theory (MFT)[35–41], cluster MFT[42, 43], the positive P representation[37, 44], the corner-space renormalization group method[45], functional renormalization group using a Keldysh path integral[32, 46], quantum trajectories[38, 43, 47], matrix-product-state based methods [48–50] and a truncated hierarchy of correlators [51]. These studies all assume a simple and decoupled form of Lindblad jump operators, i.e. $L_{i,-} = b_i$, which works well for describing nearly isolated non-interacting atoms. In general, however, such an assumption does not hold for a strongly correlated system when $\gamma_{k,k'}/U \ll 1$.

In this work, we emphasize that, the explicit form of jump operators is determined by the system Hamiltonian itself, as well as the coupling with the environment, which can significantly modify the Lindblad master equation and the properties of the steady state. In order to fully understand the phases and dynamics in these

nonequilibrium systems, it is useful to have prototypical solvable models [52]. Here we study the Bose Hubbard Hamiltonian (1) with an all-to-all hopping for N sites, i.e. $t_{ij} = t/N$ for any i, j . The all-to-all hopping mimics the effect of a mean-field analysis at the equilibrium level, and allows us to move beyond mean-field with analytical control. Remarkably, in such an approach we are able to derive the explicit form of the Lindblad jump operators, analytically obtain closed-form solutions of the steady state in certain limits, and numerically solve the system for up to thousands of sites in others.

Our main results are summarized in the phase diagram, Fig. 1, as a function of the ratio of exciton production and decay rates I_0/γ_0 and $t/(t+U)$. Similar to the equilibrium model, we see that there are two phases: Mott-insulator phases with an integer values of $n_B = (1/N) \sum_i \langle b_i^\dagger b_i \rangle$ and a superfluid phase identified as a non-zero value of $\Psi^2 = (1/N^2) \sum_{i,j} \langle b_i^\dagger b_j \rangle$ with a generic value of n_B . Although the steady-state density matrices are not of a (thermal) equilibrium form, the nonequilibrium and equilibrium phase diagram resemble each other lending credence to the qualitative understanding of the experiment as tuning the boson chemical potential. We additionally study the critical properties of the phase transition. Notably, the Mott-Mott phase transition, which is simply a level crossing at the equilibrium level, becomes a continuous phase transition and the critical exponents for the Mott-superfluid transition are distinct from their equilibrium values.

II. DERIVATION OF THE MASTER EQUATION

We will analyze the Bose-Hubbard Hamiltonian, (1) with all-to-all hopping between the N sites, $t_{i,j} = t/N$, and in the presence of coupling to the environment. We will assume that $\mu \gg U, t$ as is relevant for the physical system, where μ is the excitation gap of excitons.

We now proceed to derive the Lindblad master equation in the weak-coupling limit (2) for this model. We follow the standard procedure [53, 54]: first, we start with a general coupling form between the system and environment $H_I = \sum_\alpha S_\alpha \otimes \mathcal{R}_\alpha$, where S_α (\mathcal{R}_α) are Hermitian operators that act on the system (environment), and the index α labels different operators. Then, we decompose $S^\alpha = \sum_j S_{\alpha;j}$ by eigenoperators of the system Hamiltonian H_0 , which are defined by the relation $[H_0, S_{\alpha;j}] = -\omega_j S_{\alpha;j}$. The Lindblad jump operators are nothing but the eigenoperators $S_{\alpha;j}$, and the damping rate $\gamma_{\alpha;j}$ is given by $\int_{-\infty}^{+\infty} ds e^{i\omega_j s} \langle \mathcal{R}_\alpha^\dagger(s) \mathcal{R}_\alpha(0) \rangle$. With these operators in hand, the equation of motion for the system's density matrix can be written out explicitly according to (2).

Since the excitons emit light when they decay, we know that they interact with the quantized electromagnetic field. A typical dipole interaction takes the form $-\sum_i \vec{D}_i \cdot \vec{E}_i$, with $\vec{D}_i \sim (b_i^\dagger + b_i)$. In momentum space, af-

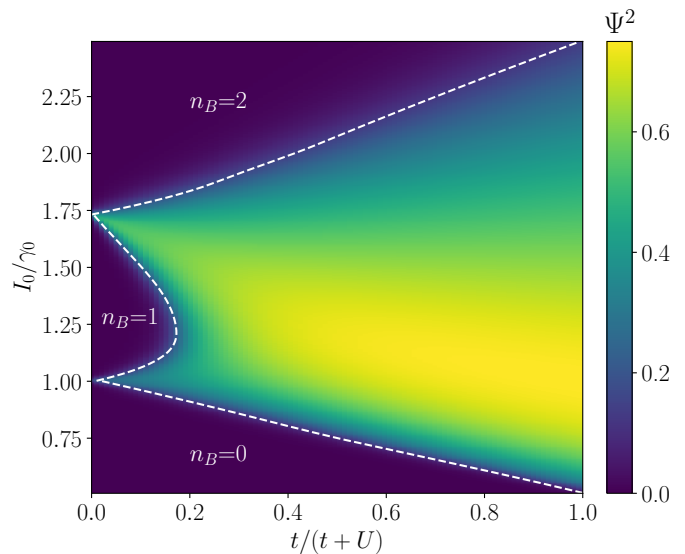


Figure 1. We plot the order parameter $\Psi^2 = \sum_{i,j} \langle b_i^\dagger b_j \rangle / N^2$ computed for the steady-state density matrix ρ_{ss} , extrapolated to the $N \rightarrow \infty$ limit as a function of the ratio of exciton production and decay rates, I_0/γ_0 , and $t/(t+U)$. $I_0(\gamma_0)$ are pumping(decay) rates at energy $\omega = \mu$. Damping rates at other energies are specified as in Sec. V. The phase boundaries are estimated using the entropy per site $S = -\text{Tr}[\rho_{ss} \ln(\rho_{ss})]/N$, which is maximal at the phase transition. We see that $n_B = 0, 1, 2$ in the lobes as indicated on the plot in the SI Appendix.

ter the rotating-wave approximation, it can be expressed as [55]

$$\sum_{\mathbf{k}, \pm} g_{\mathbf{k}, \pm} a_{\mathbf{k}, \pm} b_{\mathbf{k}}^\dagger \approx \frac{1}{\sqrt{N}} \sum_{\mathbf{k}, \pm} g_{\mathbf{k}, \pm} a_{\mathbf{k}, \pm} \sum_i b_i^\dagger \quad (3)$$

where $g_{\mathbf{k}, \pm}$ is related to the polarization of the light mode. We used $\mathbf{k} \cdot \mathbf{r}_i \ll 1$, since the relevant wavelength of light (≈ 700 nm) is much larger than the distance between moiré unit cells (≈ 7.5 nm)[56]. Therefore, as opposed to the common assumption where each site couples to different modes in the bath, we assume the environment couples with the system in a collective way, reminiscent of the Dicke model [57]. Note that $g_{\mathbf{k}} \sim \mathcal{O}(\sqrt{N/V})$ where V is the volume available to the photon modes, and we suppress the light's polarization for simplicity. With such assumption, we may write the coupling as

$$H_I = \mathcal{B}^\dagger \mathcal{R} + \mathcal{R}^\dagger \mathcal{B} \quad (4a)$$

with

$$\mathcal{B} \equiv \sum_i b_i \quad (4b)$$

where \mathcal{R} denotes the environment operator. Though we only argued above for the decay of excitons to have such a

form, treating the production and decay on equal footing allows us to make theoretical progress.

We do not specify the explicit forms of \mathcal{R} since they could be complicated in general. Specifically, the long-lived interlayer excitons which form the exciton lattice are generated through at least a two-step process, where intralayer excitons are photoexcited and then converted to interlayer excitons through some relaxation process[23]. We therefore consider only the incoherent contributions of H_I to the exciton system.

We now decompose \mathcal{B} in H_I in terms of eigenoperators, which, in general, requires diagonalizing H_0 . Note that the coupling to the environment and the Hamiltonian itself are invariant under all permutations of the sites; we also assume the system's initial state (before turning on exciton-producing effects) is the vacuum $\rho = |0\rangle\langle 0|$ since $\mu > 0$, which has permutation symmetry as well. Therefore, the only states that are accessed are in the fully symmetric sector of this permutation symmetry and it is sufficient to diagonalize H_0 in this sector.

We parametrize the sector with the normalized states

$$|\vec{n}\rangle = \frac{1}{\sqrt{N! \prod_i (n_i)!}} \sum_{\sigma \in S_N} \sigma |n_0, n_1, \dots, n_M\rangle \quad (5)$$

where \vec{n} is a vector in $(M+1)$ dimensional space, S_N is the symmetric group, σ is the permutation operator that shuffles site i to $\sigma(i)$, and the state $|n_0, n_1, \dots, n_M\rangle$ has the first n_0 sites being unoccupied, the next n_1 sites having one boson occupied, etc. We have chosen a maximum number of allowed bosons per site, M , and $\sum_i n_i = N$.

It is convenient to define transition operators $\mathcal{O}_{n,m} \equiv \sum_i |n\rangle\langle m|_i \otimes \prod_{j \neq i} \mathbb{1}_j$ which changes site i from having m bosons to n bosons and acts as the identity on all other sites. Note that $\mathcal{O}_{n,m} \sigma = \sigma \mathcal{O}_{n,m}$ for all $\sigma \in S_N$. We can then find

$$\mathcal{O}_{n,m} |\vec{n}\rangle = |\vec{n} - \hat{e}_m + \hat{e}_n\rangle \begin{cases} \sqrt{n_m(n_n + 1)} & \text{if } n \neq m \\ n_m & \text{if } n = m \end{cases} \quad (6)$$

where \hat{e}_i are the unit vectors and n_m are the components of \vec{n} .

Letting \hat{N}_B be the total boson number operator with eigenvalues N_B , we use these relations to write H_0 in the $|\vec{n}\rangle$ basis:

$$H_0 |\vec{n}\rangle = (\mu N_B + \frac{U}{2} \sum_n n(n-1)n_n) |\vec{n}\rangle - \frac{t}{N} \sum_{nm} \sqrt{nm n_m n_{m-1}^{(m)} n_{n-1}^{(m)} (n_n^{(m)} + 1)} |\vec{n}^{(m)} - \hat{e}_{n-1} + \hat{e}_n\rangle \quad (7)$$

where $\vec{n}^{(m)} = \vec{n} - \hat{e}_m + \hat{e}_{m-1}$. For a given M and N , we can numerically find the eigenbasis within each N_B sector where only the ratio t/U determines the eigenvectors. We denote the eigenvectors $|\alpha, N_B\rangle$ where each sector has a different number of allowed α .

We now eigen-decompose the coupling operator $\mathcal{B} = \sum_i b_i$ within the fully-permutation-symmetric sector to

find:

$$\mathcal{B} = \sum_{\lambda} \mathcal{B}_{\lambda} = \sum_{(\alpha, \beta, N_B)} B_{(\alpha, \beta, N_B)} |\alpha, N_B - 1\rangle \langle \beta N_B|.$$

where $B_{(\alpha, \beta, N_B)} = \langle \alpha, N_B - 1 | \mathcal{B} | \beta N_B \rangle$ and $\lambda = (\alpha, \beta, N_B)$ is a combined index. Note that the operators in the sum have energy $[H, |\alpha, N_B - 1\rangle \langle \beta N_B|] = -(E_{\beta, N_B} - E_{\alpha, N_B - 1}) |\alpha, N_B - 1\rangle \langle \beta N_B| = -\omega_{\alpha, \beta, N_B} |\alpha, N_B - 1\rangle \langle \beta N_B|$.

With the eigenoperators in hand, we can immediately write out the interaction-picture Lindblad equation (ignoring the Lamb shift)

$$\begin{aligned} \dot{\rho}(t) = & \sum_{\lambda, \lambda': \omega_{\lambda} = \omega_{\lambda'}} \gamma(\omega_{\lambda}) \mathcal{L}(B_{\lambda}(\omega_{\lambda}), B_{\lambda'}^{\dagger}(\omega_{\lambda'})) [\rho(t)] \\ & + \sum_{\lambda, \lambda': \omega_{\lambda} = \omega_{\lambda'}} I(\omega_{\lambda}) \mathcal{L}(B_{\lambda}^{\dagger}(\omega_{\lambda}), B_{\lambda'}(\omega_{\lambda'})) [\rho(t)]. \end{aligned} \quad (8)$$

The first (second) line corresponds to decay (pumping) processes. Equality between ω_{λ} and $\omega_{\lambda'}$ is determined by the condition $|\omega_{\lambda} - \omega_{\lambda'}| \ll \tau^{-1}$, where τ sets the relaxation timescale of the system. The specifics of the environment enter only through

$$\begin{aligned} \gamma(\omega) &= \int_{-\infty}^{\infty} ds e^{i\omega s} \langle \mathcal{R}(s) \mathcal{R}^{\dagger} \rangle \\ I(\omega) &= \int_{-\infty}^{\infty} ds e^{-i\omega s} \langle \mathcal{R}(s) \mathcal{R} \rangle \end{aligned} \quad (9)$$

and we have assumed $\langle \mathcal{R}(s) \mathcal{R} \rangle = \langle \mathcal{R}^{\dagger}(s) \mathcal{R}^{\dagger} \rangle = 0$ (and τ^{-1} is set by $\gamma(\omega), I(\omega)$ which are assumed to be the smallest energy scales in the weak-coupling limit).

We now write out (8) in the eigenbasis, $|\alpha, N_B\rangle$. One difficulty in solving the resulting equation is the presence of coherences (i.e. off-diagonal terms of the density matrix in the basis of energy eigenstates). As we derive in the SI Appendix, the Lindblad master equation can only generate coherences within energy-degenerate sectors, and therefore, if there is no degeneracy, the steady-state density matrix is diagonal. However, there is a weaker condition that ensures that the $\mathcal{B}_{\lambda}(\omega_{\lambda})$ operators never generate coherences when acting on a diagonal ρ (see SI Appendix): $\omega_{\alpha, \beta, N_B} = \omega_{\alpha', \beta, N_B}$ ($\omega_{\alpha, \beta, N_B} = \omega_{\alpha, \beta', N_B}$) only when $B_{(\alpha, \beta, N_B)} = 0$ or $B_{(\alpha', \beta, N_B)} = 0$ ($B_{(\alpha, \beta, N_B)} = 0$ or $B_{(\alpha, \beta', N_B)} = 0$), respectively. In our analytic or numerical results, we always check that the above condition is satisfied for this system.

We can therefore write $\rho = \sum_{\alpha, N_B} \rho_{\alpha, N_B} |\alpha, N_B\rangle \langle \alpha, N_B|$ and

$$\begin{aligned} \dot{\rho}_{a, N_B} = & \sum_{\lambda=(\alpha, a, N_B)} |B_{\lambda}|^2 (I(\omega_{\lambda}) \rho_{\alpha, N_B - 1} - \gamma(\omega_{\lambda}) \rho_{a, N_B}) \\ & + \sum_{\lambda=(a, \beta, N_B + 1)} |B_{\lambda}|^2 (\gamma(\omega_{\lambda}) \rho_{\beta, N_B + 1} - I(\omega_{\lambda}) \rho_{a, N_B}). \end{aligned} \quad (10)$$

As a check on our derivation, we can set $I(\omega)$ and $\gamma(\omega)$ to represent a thermal bath of free bosons. In this case,

$\gamma(\omega) = A(\omega)(1 + n_B(\omega/T))$ and $I(\omega) = A(\omega)n_B(\omega/T)$ where $A(\omega)$ is a function only of ω , $n_B(x) = (e^x - 1)^{-1}$ is the Bose-Einstein distribution. We numerically find that the steady-state density matrix, $\dot{\rho}_{a,N_B} = 0$ has the thermal form $\rho_{a,N_B} \sim e^{-E_{a,N_B}/T}$. In general, we consider non-zero $I(\omega)$ as resulting from light-induced, rather than thermal, production of excitons.

III. KEY OBSERVABLES, PHASES, AND EXPONENTS

Once the steady state satisfying $\dot{\rho}_{a,N_B} = 0$ from (10) is determined, there are two key observables to evaluate:

$$n_B = \frac{1}{N} \sum_i \langle b_i^\dagger b_i \rangle, \quad \Psi^2 = \frac{1}{N^2} \sum_{i,j} \langle b_i^\dagger b_j \rangle = \frac{\langle \mathcal{B}^\dagger \mathcal{B} \rangle}{N^2}. \quad (11)$$

The two phases present in our model are Mott-insulating phases with integer exciton density $n_B \in \{0, 1, 2, \dots\}$ (and $\Psi^2 = 0$) and a superfluid phase with generic n_B and $\Psi^2 \neq 0$. In the equilibrium case, the superfluid phase is determined by the non-zero expectation $\langle b_i \rangle$ (or equivalently the long-range order of $\langle b_i^\dagger b_j \rangle$), and Ψ^2 is our analogous observable.

In addition to the phases themselves, we study the phase transitions and extract the critical exponents. We will tune across the phase transitions primarily by adjusting the ratio $r(\omega) = I(\omega)/\gamma(\omega)$ of the exciton production and decay strengths. With $\mu \gg U, t$, we may Taylor expand $r(\omega)$ around $\omega = \mu$ and the transition occurs when $r(\mu) = r_1$ reaches a critical value r_c .

At a continuous phase transition, there is an order parameter χ that takes a particular form close to the phase transition

$$\chi = \begin{cases} \chi_0(r_1 - r_c)^\beta & r_1 > r_c \\ 0 & r_1 < r_c \end{cases}, \quad (12)$$

where χ_0 is a constant, and the correlation length ξ of the system will diverge as $\xi \sim (r_1 - r_c)^{-\nu}$. The exponents β and ν are universal numbers set by the phase transition itself, independent of the exact microscopic model. For systems of a finite length L , this diverging correlation length leads to the finite-size scaling form for $\chi = L^{-\beta/\nu} f_\chi(L^{1/\nu}(r_1 - r_c))$, where $f_\chi(x)$ is a finite-size scaling function [58].

The all-to-all hopping in our system makes it difficult to define a correlation length, so we define the exponent λ as the analog for ν in our system. At the Mott-Mott transition from the $n_B = 0$ to $n_B = 1$ Mott phases, the order parameter is simply n_B , which therefore has the form

$$n_B = N^{-\beta_m/\lambda_m} f_{n_B,m}(N^{1/\lambda_m}(r_1 - r_c)) \quad (13)$$

where β_m , λ_m are the critical exponents and $f_{n_B,m}(x)$ is the scaling function for n_B at the Mott-Mott transition.

Similarly, at the Mott-superfluid (Mott-Mott) transition, the order parameter is Ψ^2 and takes the scaling form

$$\Psi^2 = N^{-\beta_s/\lambda_s} f_{\Psi^2,s}(N^{1/\lambda_s}(r_1 - r_c)) \quad (14)$$

with similarly defined β_s , λ_s and $f_{\Psi^2,s}(x)$. Note that the exponents λ_m/s and β_m/s and scaling functions do not depend on the exact definition of the tuning parameter used to move between the two phases, and they can distinguish between different critical points.

IV. ANALYTIC RESULTS

Due to needing to find the eigenvectors of H_0 , (7), we cannot make additional analytic progress in most cases. We will treat the general problem numerically in the next section, but there are two cases where more analytic progress can be made¹.

A. $t = 0$

In this limit, the eigenvectors of H_0 are simply the $|\vec{n}\rangle$ states defined above. Instead of simplifying (10), we note that

$$\mathcal{B} = \sum_{j=1}^M \sqrt{j} \mathcal{O}_{j-1,j} \quad (15)$$

and $[H, \mathcal{O}_{j-1,j}] = -[\mu + U(j-1)]\mathcal{O}_{j-1,j} = -\omega_j \mathcal{O}_{j-1,j}$. We can therefore write out the equivalent of (8)

$$\begin{aligned} \dot{\rho}(t) = & \sum_j \gamma(\omega_j) j \mathcal{L} \left(\mathcal{O}_{j-1,j}, \mathcal{O}_{j-1,j}^\dagger \right) [\rho(t)] \\ & + \sum_j I(\omega_j) j \mathcal{L} \left(\mathcal{O}_{j-1,j}^\dagger, \mathcal{O}_{j-1,j} \right) [\rho(t)]. \end{aligned} \quad (16)$$

We now substitute $\rho = \sum_{\vec{n}, \vec{m}} \rho_{\vec{n}, \vec{m}} |\vec{n}\rangle \langle \vec{m}|$. Using (6) and the fact that we start from a vacuum state, one can check that the condition $\rho_{\vec{n}, \vec{m}} = 0$ when $\vec{n} \neq \vec{m}$, is preserved under time evolution. Therefore, we may instead write $\rho(t) = \sum_{\vec{n}} \rho_{\vec{n}}(t) |\vec{n}\rangle \langle \vec{n}|$.

We can explicitly write out the steady-state equation as

$$\begin{aligned} 0 = & \sum_{j=1}^M j n_{j-1} (n_j + 1) (\gamma(\omega_j) \rho_{\vec{n} - \hat{e}_{j-1} + \hat{e}_j} - I(\omega_j) \rho_{\vec{n}}) \\ & + \sum_{j=1}^M j n_j (n_{j-1} + 1) (I(\omega_j) \rho_{\vec{n} - \hat{e}_j + \hat{e}_{j-1}} - \gamma(\omega_j) \rho_{\vec{n}}) \end{aligned} \quad (17)$$

¹ We additionally consider $U = 0$ in the SI Appendix but our formalism must be slightly modified to admit a consistent calculation.

where the above equation holds for all \vec{n} and n_j denote components of \vec{n} . A sufficient ‘‘detailed-balance’’-like condition for the steady-state is that all terms in the sum are zero,

$$\gamma(\omega_j)\rho_{\vec{n}-\hat{e}_{j-1}+\hat{e}_j} = I(\omega_j)\rho_{\vec{n}}, \quad (18)$$

which remarkably specifies the solution in this case. (In general, the equivalent set of equations will not hold as they overdetermine the solution.) It can easily be checked that the steady-state is given explicitly as

$$\rho_{\vec{n}} = \rho_0 \prod_{i=1}^M \left(\prod_{j=1}^i \frac{I(\omega_j)}{\gamma(\omega_j)} \right)^{n_i} = \rho_0 \prod_{i=1}^M (r(\omega_i))^{\sum_{j=i}^M n_j} \quad (19)$$

where we have defined $r(\omega_j) \equiv I(\omega_j)/\gamma(\omega_j) = r_j$. This form of the steady-state manifestly reveals that we can set the maximum number of bosons per site we need to consider, M , by the condition $r(\omega_M) \ll 1$, when $t = 0$.

We now analyze the case $M = 2$ in detail: We can rewrite the density matrix as $\rho_{\vec{n}} = \rho_0 r_1^{n_1} (r_1 r_2)^{n_1 + n_2}$ (and we assume that $r_j > r_{j+1}$). We can compute the average number of bosons per site $n_B = \langle N_B \rangle / N$ as

$$n_B = \begin{cases} 0 + \frac{1}{N} \frac{r_1 + (2-3r_1)r_1 r_2}{(r_1-1)(r_1 r_2-1)} + \dots & \text{if } r_1^N, r_2^N \ll 1 \\ 1 + \frac{1}{N} \frac{1-r_1 r_2}{(r_1-1)(r_2-1)} + \dots & \text{if } r_1^{-N}, r_2^N \ll 1 \\ 2 + \frac{1}{N} \frac{3-2r_2-r_1 r_2}{(r_2-1)(r_1 r_2-1)} + \dots & \text{if } r_1^N, r_2^N \gg 1. \end{cases} \quad (20)$$

We can see, in the thermodynamic limit, that our model has a sharp transition from an $n_B = 0$ to $n_B = 1$ to $n_B = 2$ state as we increase the ratio r_1 and r_2 . We identify these regions as Mott-insulators (and we can numerically check that $\Psi^2 \rightarrow 0$). We can analyze these critical points by evaluating

$$n_B = \begin{cases} \frac{1}{2} + \frac{1}{12}(r_1 - 1)N + \dots & \text{if } r_1 \approx 1, r_2^N \ll 1 \\ \frac{3}{2} + \frac{1}{12}(r_2 - 1)N + \dots & \text{if } r_2 \approx 1, r_1^N \gg 1 \end{cases} \quad (21)$$

implying that n_B has the scaling form $n_B = N^{-\beta_m/\lambda_m} f_{n_B, m}(N^{1/\lambda_m}(r_j - 1))$ with $\lambda_m = 1$ and $\beta_m = 0$. We expect that the values of λ_m, β_m are insensitive to increasing M .

In equilibrium, this transition is first order, since it is simply a level crossing of the two competing ground states, $|N\hat{e}_j\rangle$ to $|N\hat{e}_{j+1}\rangle$. However, in the nonequilibrium setting, as we approach the phase transition there are more and more states in the Hilbert space that contribute to the steady-state density matrix, which allows for a continuous phase transition to emerge between $\rho_{ss} \approx |N\hat{e}_j\rangle\langle N\hat{e}_j|$ to $\rho_{ss} \approx |N\hat{e}_{j+1}\rangle\langle N\hat{e}_{j+1}|$.

B. $M = 1$

If we consider the case of hardcore bosons, i.e. $U \rightarrow \infty$, we can make additional progress as well because there is only one state per (fully symmetrized) sector, N_B , and

therefore the eigenstates of H_0 can be specified as $|N_B\rangle$. The eigenenergy of the states is given by

$$E_{N_B} = \mu N_B - \frac{t}{N} N_B(N - N_B + 1) \quad (22)$$

and we can evaluate

$$\mathcal{B} = \sum_{N_B=1}^N \sqrt{N_B(N - N_B + 1)} |N_B - 1\rangle\langle N_B| \quad (23)$$

so $B_\lambda = B_{N_B} = \sqrt{N_B(N - N_B + 1)}$ and these have energies $\omega_{N_B} = E_{N_B} - E_{N_B-1} = \mu - t(1 - 2(N_B - 1)/N)$. When t is non-zero, we see that the energy will take on a range of values from $\mu - |t| < \omega < \mu + |t|$ in the thermodynamic limit.

Since all ω_{N_B} are unique, we still have no coherences and can write down the density matrix equation

$$\begin{aligned} \dot{\rho}_m &= m(N - m + 1)(I(\omega_m)\rho_{m-1} - \gamma(\omega_m)\rho_m) \\ &\quad + (m + 1)(N - m)(\gamma(\omega_{m+1})\rho_{m+1} - I(\omega_{m+1})\rho_m) \end{aligned} \quad (24)$$

where m is specifying N_B . Again noting that a sufficient condition for the steady-state solution is

$$\gamma(\omega_m)\rho_m = I(\omega_m)\rho_{m-1} \quad (25)$$

we find

$$\rho_m = \rho_0 \prod_{j=1}^m \frac{I(\omega_j)}{\gamma(\omega_j)} = \rho_0 \prod_{j=1}^m r(\omega_j) \quad (26)$$

If $t = 0$, we see that $\omega_m = \mu$ for all m , so we quickly derive (19) for $M = 1$.

We will now show that, in addition to the $n_B = 0$ and $n_B = 1$ Mott phases seen before, there is an intermediate phase. We first assume the pump-to-decay ratio $r(\omega_j) = r_j$ decreases monotonically with ω , which fits the intuition that higher energy excitations are prone to decay more quickly. Defining $r_< \equiv r(\mu - t)$ [$r_> \equiv r(\mu + t)$], we can recover the Mott phases from before by computing $\rho_m = \rho_0 r_<^m e^{(r_<^2 t m^2)/(r_< N)}$ [$\rho_{N-m} = \rho_0 r_>^{-m} e^{(r_>^2 t m^2)/(r_> N)}$] when $r_< \ll 1$ ($r_> \gg 1$), respectively, where $r'_{< / >}$ are the corresponding values of $r'(\omega) = dr(\omega)/d\omega < 0$ (see SI Appendix for additional calculation details for this section).

Next, we consider the case $r_< > 1 > r_>$. There then exists some index j^* where $r_{j^*} = 1$. From (25) and (26), we can find as $N \rightarrow \infty$

$$\rho_{j^* \pm m} \approx \rho_{j^*} e^{-\delta m^2} \quad (27)$$

where $\delta = -r'_{j^*} t / N > 0$ from the monotonic decrease assumption.

We can deduce this density matrix represents an additional phase by measuring Ψ^2 . Since $M = 1$, we see that $\mathcal{B}^\dagger \mathcal{B} |N_B\rangle = N_B(N - N_B + 1) |N_B\rangle$. In the three aforementioned limits, we find

$$\Psi^2 = \begin{cases} \frac{r_{<}}{N}(1-r_{<})^{-1} + \dots & \text{if } r_{<} \ll 1 \\ \frac{j^*}{N} \left(1 - \frac{j^*}{N}\right) + \dots & \text{if } r_{j^*} = 1 \text{ and } j^* \sim O(N) \\ \frac{1}{N}(1-r_{>}^{-1})^{-1} + \dots & \text{if } r_{>} \gg 1 \end{cases} \quad (28)$$

As above, we can observe a critical scaling emerge as $r_{<} \rightarrow 1$. Using (26), we can find

$$\Psi^2 \approx \frac{1}{N^{1/2}} \frac{\int_0^\infty dx x \exp\left[\frac{r'_{<} t}{r_{<}} x^2 - (1-r_{<})\sqrt{N}x\right]}{\int_0^\infty dx \exp\left[\frac{r'_{<} t}{r_{<}} x^2 - (1-r_{<})\sqrt{N}x\right]}. \quad (29)$$

which has the scaling form $\Psi^2 = N^{-1/2} f_{\Psi^2,s}(N^{1/2}(r_{<} - 1))$, implying that $\lambda_s = 2$ and $\beta_s = 1$. A similar finite-size scaling form, with the same value of λ_s , can be derived for n_B .

V. NUMERICAL RESULTS

From the analytic results, we can see there are two phases distinguished by Ψ^2 . If $\Psi^2 \rightarrow 0$, then we are in a Mott insulating phase where n_B is approximately an integer. Otherwise, n_B takes an intermediate value and Ψ^2 is non-zero, like in the superfluid phase. By solving the system numerically, we can explore what happens when $t \neq 0$ and more than one boson per site is allowed.

In order to proceed numerically, we must specify $I(\omega)$ and $\gamma(\omega)$. We take $\gamma(\omega) = \gamma_0(\omega/\mu)^3$, the correct form for photon-driven decay, and we assume $I(\omega) = I_0$ for simplicity². For the moiré TMD system [27], the realistic excitation gap $\mu \approx 1.5$ eV and the repulsion $U \approx 30$ meV. However, we fix $\mu = 150$ meV as μ only affects $\gamma'(\omega)$ [and consequently $r'(\omega)$] which we need to be large to achieve numerical convergence. We let $(t + U)$ set the energy scale, and vary both $t/(t + U)$ and $r(\mu) = I_0/\gamma_0$ to map out the phase diagram and study the critical exponents.

Once $t \neq 0$ and $M \geq 2$, we can only numerically determine the Lindblad operators and energy eigenstates, and the equivalent conditions to (18) and (25) cannot all be satisfied. Instead, we construct the Liouvillian super-operator \mathcal{L} satisfying $\dot{\rho} = \mathcal{L}\rho$ from (10) and search for the steady-state ρ that has eigenvalue zero. We can numerically evaluate the $M = 2$ case up to large system size of $N \sim 1000$. In this case, when $t = 0$, the various N_B sectors are non-degenerate implying that the steady-state density matrix is diagonal, as we argued above. We check numerically that this non-degeneracy persists when $t \neq 0$.

In addition to measuring n_B and Ψ^2 , we measure the entropy $S = -\text{Tr}[\rho \ln(\rho)]$ and the Liouvillian gap, $\Delta_{\mathcal{L}}$

determined from the smallest real part of any of the non-zero eigenvalues of \mathcal{L} [59]. These two quantities allow us to better distinguish between the two phases and characterize their critical behavior numerically. We extrapolate these quantities to the $N \rightarrow \infty$ limit (see SI Appendix).

In Fig. 1, we observe the same two phase as above: the Mott phase is signified by integer n_B with $\Psi^2 = 0$ and $S/N = 0$, and the superfluid phase is signified by generic n_B and $\Psi^2 \neq 0$. At the phase boundary, S/N attains a maximum, clearly demarcating the two phases. The phase diagram in Fig. 1 qualitatively matches the equilibrium phase diagram with its $n_B = 1$ Mott lobe. If $M > 2$, then we would see additional Mott lobes as well (see SI Appendix).

In addition to mapping out the phase diagram, we can confirm the universal scaling forms discussed above. In Fig. 2(a), at the transition between two Mott phases, we observe that $n_B = f_{n_B,m}(N(I_0 - I_0^c))$, as expected from (13), indicating that $\lambda_m = \beta_m + 1 = 1$. Within the equilibrium phase diagram, this transition is first order (a level crossing) indicating that the environment can change the nature of the critical point. In Fig. 2(b), we similarly see $\Psi^2 = N^{-1/2} f_s(N^{1/2}(I_0 - I_0^c))$, as above, for a transition between the Mott and superfluid phase with $\lambda_s = 2$ and $\beta_s = 1$, as opposed to the equilibrium values of $\lambda_s = \beta_s = 1$ (see SI Appendix). We confirm that the same exponents are extracted while tuning t/U instead of I_0/γ_0 across the phase transition.

Finally, when $M = 1$, we can extract the Liouvillian gap, $\Delta_{\mathcal{L}}$. Away from the critical point, $\Delta_{\mathcal{L}}/N$ approaches a constant indicating an effect similar to super-radiance [54]. At criticality, however, we find $\Delta_{\mathcal{L}}/N \sim N^{-1/\lambda}$, indicating a critical slowing down (i.e. a longer time to reach the steady state) near the phase boundary (see Fig. S7 in the SI Appendix). We expect that this same behavior should arise at the phase transitions when $M \geq 2$, but we are unable to compute $\Delta_{\mathcal{L}}$ for large enough system sizes.

VI. DISCUSSION AND CONCLUSION

We have introduced a solvable variant of the Bose Hubbard model coupled to an environment. We find two phases that resemble the equilibrium Mott and superfluid phases, but the density matrix does not take a Boltzmann form [(27)]. We extract critical exponents $\lambda_m = \beta_m + 1 = 1$ ($\lambda_s = \beta_s + 1 = 2$) for the transition between a Mott phase and a Mott (superfluid) phase, respectively. These exponents are different from the observed equilibrium exponents derived in the SI Appendix (and the Mott-Mott transition is first-order in equilibrium). The change in criticality is not surprising—although previous work found that the open system criticality can only change a dynamic exponent [32, 46], universality is typically only insensitive to local perturbations, and the environment acts as a global perturbation.

We derive the Lindblad operators and master equa-

² The realistic $I(\omega)$ would require sophisticated modeling since the excitons are generated through complicated pump and relaxation processes.

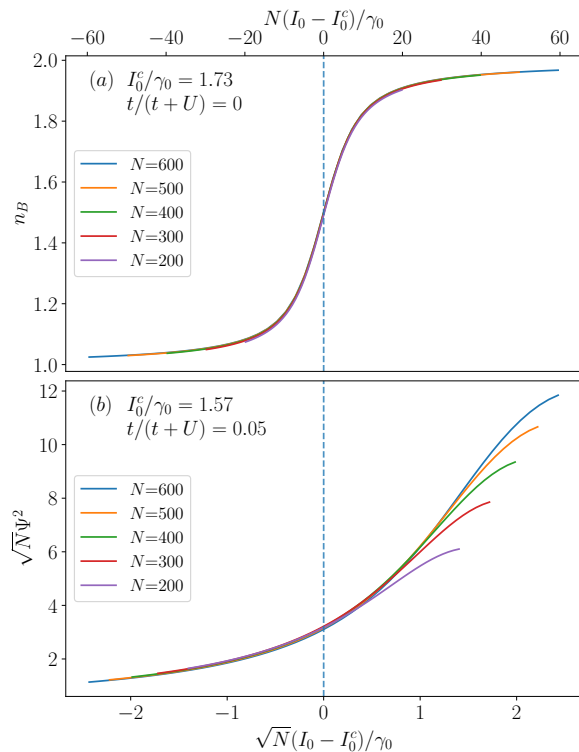


Figure 2. We perform scaling collapses for the order parameters at the (a) transition between the $n_B = 1$ and $n_B = 2$ Mott phases and (b) transition between Mott and superfluid phases. The $N \rightarrow \infty$ curve that the different data collapses onto in (a) [(b)], are, respectively, the $f_{n_B, m}(x)$ [$f_{\Psi^2, s}(x)$] defined in the text. We find that $\lambda_m = 1$ and $\beta_m = 0$ for the former and $\lambda_s = 2 = \beta_s + 1$ for the latter. We have confirmed that this exponent stays the same regardless of which Mott lobes are involved and regardless of whether we tune I_0/γ_0 or t/U .

tions from an explicit form of the coupling between the system and environment. Our model is solvable because the environment couples in a site-invariant way that allows us to only consider the fully symmetric sector of the permutation group, and the calculation is controlled by $1/N$ for large system size. We note that, although the full eigensystem information of H_S is difficult to obtain, only the eigenstates that are connected by the derived

Lindblad operators are relevant, and we demonstrate this idea in the SM for the case $U/t = 0$ in the SI Appendix. For generic t/U , it may be possible to obtain Lindblad operators perturbatively controlled by $1/N$, but we leave this work for the future.

Our formulation of site-invariant coupling between the system and its environment is reminiscent of the Dicke model [57] and will display superradiance [54]. However, since we model the production as the reverse process of decay, our model also has superabsorption. This observation explains why, when $I < \gamma$, the steady state has only a finite number of excitons in the thermodynamic limit: if the production rate I is less than the decay rate γ , an extensive number of excitons cannot be built up.

In the experimental systems [27–31], there may be an additional local coupling $H'_I = \sum_i b_i^\dagger \mathcal{R}'_i + \text{h.c.}$ responsible for the production of the bosons, but introducing such a term into our formalism would destroy the solvability. Future work should consider the competition between a local production of bosons and their global (or longer-range) decay, as well as a short-range hopping system Hamiltonian, which might be resolved by numerical methods such as dynamical mean-field theory.

ACKNOWLEDGMENTS

We thank Chenhao Jin and Richen Xiong for discussing their experiments. We thank Matthew Fisher for helpful discussions. LB and ZS are supported by the NSF CMMT program under Grant No. DMR-2419871. TC is supported by a University of California Presidential Postdoctoral Fellowship and acknowledges support from the Gordon and Betty Moore Foundation through Grant No. GBMF8690 to UCSB. This research was supported by the Simons Collaboration on Ultra-Quantum Matter, which is a grant from the Simons Foundation (Grant No. 651440), and, in part, by grant NSF PHY-2309135 to the Kavli Institute for Theoretical Physics (KITP). Use was made of the computational facilities administered by the Center for Scientific Computing at the CNSI and MRL (an NSF MRSEC; DMR-1720256) and purchased through NSF CNS-1725797.

* These authors contributed equally to this work

- [1] M. P. A. Fisher, P. B. Weichman, G. Grinstein, and D. S. Fisher, Boson localization and the superfluid-insulator transition, *Phys. Rev. B* **40**, 546 (1989).
- [2] Y. Takasu, T. Yagami, H. Asaka, Y. Fukushima, K. Nagao, S. Goto, I. Danshita, and Y. Takahashi, Energy redistribution and spatiotemporal evolution of correlations after a sudden quench of the bose-hubbard model, *Science advances* **6**, eaba9255 (2020).
- [3] M. Endres, M. Cheneau, T. Fukuhara, C. Weitenberg,

- P. Schauß, C. Gross, L. Mazza, M. C. Bañuls, L. Pollet, and I. Bloch, Observation of correlated particle-hole pairs and string order in low-dimensional mott insulators, *Science* **334**, 200 (2011).
- [4] B. Yang, H. Sun, R. Ott, H.-Y. Wang, T. V. Zache, J. C. Halimeh, Z.-S. Yuan, P. Hauke, and J.-W. Pan, Observation of gauge invariance in a 71-site bose-hubbard quantum simulator, *Nature* **587**, 392 (2020).
- [5] G.-X. Su, H. Sun, A. Hudomal, J.-Y. Desaulles, Z.-Y. Zhou, B. Yang, J. C. Halimeh, Z.-S. Yuan, Z. Papić, and

- J.-W. Pan, Observation of many-body scarring in a bose-hubbard quantum simulator, *Phys. Rev. Res.* **5**, 023010 (2023).
- [6] M. Greiner, O. Mandel, T. Esslinger, T. W. Hänsch, and I. Bloch, Quantum phase transition from a superfluid to a mott insulator in a gas of ultracold atoms, *nature* **415**, 39 (2002).
- [7] C. Noh and D. G. Angelakis, Quantum simulations and many-body physics with light, *Reports on Progress in Physics* **80**, 016401 (2016).
- [8] I. Carusotto and C. Ciuti, Quantum fluids of light, *Rev. Mod. Phys.* **85**, 299 (2013).
- [9] D. Ballarini and S. De Liberato, Polaritonics: from microcavities to sub-wavelength confinement, *Nanophotonics* **8**, 641 (2019).
- [10] A. A. Houck, H. E. Türeci, and J. Koch, On-chip quantum simulation with superconducting circuits, *Nature Physics* **8**, 292 (2012).
- [11] J. Raftery, D. Sadri, S. Schmidt, H. E. Türeci, and A. A. Houck, Observation of a dissipation-induced classical to quantum transition, *Phys. Rev. X* **4**, 031043 (2014).
- [12] A. J. Hoffman, S. J. Srinivasan, S. Schmidt, L. Spietz, J. Aumentado, H. E. Türeci, and A. A. Houck, Dispersive photon blockade in a superconducting circuit, *Phys. Rev. Lett.* **107**, 053602 (2011).
- [13] J. Fink, M. Göppl, M. Baur, R. Bianchetti, P. J. Leek, A. Blais, and A. Wallraff, Climbing the jaynes-cummings ladder and observing its nonlinearity in a cavity qed system, *Nature* **454**, 315 (2008).
- [14] S. M. Spillane, G. S. Pati, K. Salit, M. Hall, P. Kumar, R. G. Beausoleil, and M. S. Shahriar, Observation of nonlinear optical interactions of ultralow levels of light in a tapered optical nanofiber embedded in a hot rubidium vapor, *Phys. Rev. Lett.* **100**, 233602 (2008).
- [15] M. Fitzpatrick, N. M. Sundaesan, A. C. Y. Li, J. Koch, and A. A. Houck, Observation of a dissipative phase transition in a one-dimensional circuit qed lattice, *Phys. Rev. X* **7**, 011016 (2017).
- [16] T. Fink, A. Schade, S. Höfling, C. Schneider, and A. Imamoglu, Signatures of a dissipative phase transition in photon correlation measurements, *Nature Physics* **14**, 365 (2018).
- [17] S. R. K. Rodriguez, W. Casteels, F. Storme, N. Carlon Zambon, I. Sagnes, L. Le Gratiet, E. Galopin, A. Lemaître, A. Amo, C. Ciuti, and J. Bloch, Probing a dissipative phase transition via dynamical optical hysteresis, *Phys. Rev. Lett.* **118**, 247402 (2017).
- [18] V. Goblot, B. Rauer, F. Vicentini, A. Le Boité, E. Galopin, A. Lemaître, L. Le Gratiet, A. Harouri, I. Sagnes, S. Ravets, C. Ciuti, A. Amo, and J. Bloch, Nonlinear polariton fluids in a flatband reveal discrete gap solitons, *Phys. Rev. Lett.* **123**, 113901 (2019).
- [19] A. V. Gorshkov, J. Otterbach, M. Fleischhauer, T. Pohl, and M. D. Lukin, Photon-photon interactions via rydberg blockade, *Phys. Rev. Lett.* **107**, 133602 (2011).
- [20] T. Peyronel, O. Firstenberg, Q.-Y. Liang, S. Hofferberth, A. V. Gorshkov, T. Pohl, M. D. Lukin, and V. Vuletić, Quantum nonlinear optics with single photons enabled by strongly interacting atoms, *Nature* **488**, 57 (2012).
- [21] I. Carusotto, D. Gerace, H. E. Türeci, S. De Liberato, C. Ciuti, and A. Imamoglu, Fermionized photons in an array of driven dissipative nonlinear cavities, *Phys. Rev. Lett.* **103**, 033601 (2009).
- [22] A. R.-P. Montblanch, D. M. Kara, I. Paradisanos, C. M. Purser, M. S. Feuer, E. M. Alexeev, L. Stefan, Y. Qin, M. Blei, G. Wang, *et al.*, Confinement of long-lived interlayer excitons in ws2/wse2 heterostructures, *Communications Physics* **4**, 119 (2021).
- [23] P. Rivera, J. R. Schaibley, A. M. Jones, J. S. Ross, S. Wu, G. Aivazian, P. Klement, K. Seyler, G. Clark, N. J. Ghimire, *et al.*, Observation of long-lived interlayer excitons in monolayer mose2-wse2 heterostructures, *Nature communications* **6**, 6242 (2015).
- [24] A. Camacho-Guardian and N. R. Cooper, Moiré-induced optical nonlinearities: Single- and multiphoton resonances, *Phys. Rev. Lett.* **128**, 207401 (2022).
- [25] C. Lagoin, U. Bhattacharya, T. Grass, R. Chhajlany, T. Salamon, K. Baldwin, L. Pfeiffer, M. Lewenstein, M. Holzmann, and F. Dubin, Extended bose-hubbard model with dipolar excitons, *Nature* **609**, 485 (2022).
- [26] M. Müller, S. Diehl, G. Pupillo, and P. Zoller, Engineered open systems and quantum simulations with atoms and ions, in *Advances in Atomic, Molecular, and Optical Physics*, Vol. 61 (Elsevier, 2012) pp. 1–80.
- [27] R. Xiong, J. H. Nie, S. L. Brantly, P. Hays, R. Sailus, K. Watanabe, T. Taniguchi, S. Tongay, and C. Jin, Correlated insulator of excitons in wse2/ws2 moiré superlattices, *Science* **380**, 860 (2023).
- [28] H. Park, J. Zhu, X. Wang, Y. Wang, W. Holtzmann, T. Taniguchi, K. Watanabe, J. Yan, L. Fu, T. Cao, *et al.*, Dipole ladders with large hubbard interaction in a moiré exciton lattice, *Nature Physics* **19**, 1286 (2023).
- [29] Z. Lian, Y. Meng, L. Ma, I. Maity, L. Yan, Q. Wu, X. Huang, D. Chen, X. Chen, X. Chen, *et al.*, Valley-polarized excitonic mott insulator in ws2/wse2 moiré superlattice, *Nature Physics* **20**, 34 (2024).
- [30] B. Gao, D. G. Suárez-Forero, S. Sarkar, T.-S. Huang, D. Session, M. J. Mehrabad, R. Ni, M. Xie, P. Upadhyay, J. Vannucci, *et al.*, Excitonic mott insulator in a bose-fermi-hubbard system of moiré ws2/wse2 heterobilayer, *Nature Communications* **15**, 2305 (2024).
- [31] R. Xiong, S. L. Brantly, K. Su, J. H. Nie, Z. Zhang, R. Banerjee, H. Ruddick, K. Watanabe, T. Taniguchi, S. A. Tongay, *et al.*, Tunable exciton valley-pseudospin orders in moiré superlattices, *Nature Communications* **15**, 4254 (2024).
- [32] L. M. Sieberer, S. D. Huber, E. Altman, and S. Diehl, Nonequilibrium functional renormalization for driven-dissipative bose-einstein condensation, *Phys. Rev. B* **89**, 134310 (2014).
- [33] A. Biella, F. Storme, J. Lebreuilly, D. Rossini, R. Fazio, I. Carusotto, and C. Ciuti, Phase diagram of incoherently driven strongly correlated photonic lattices, *Phys. Rev. A* **96**, 023839 (2017).
- [34] J. Lebreuilly, M. Wouters, and I. Carusotto, Towards strongly correlated photons in arrays of dissipative nonlinear cavities under a frequency-dependent incoherent pumping, *Comptes Rendus Physique* **17**, 836 (2016).
- [35] F. Caleffi, M. Capone, and I. Carusotto, Collective excitations of a strongly correlated nonequilibrium photon fluid across the insulator-superfluid phase transition, *Phys. Rev. Lett.* **131**, 193604 (2023).
- [36] A. Le Boité, G. Orso, and C. Ciuti, Steady-state phases and tunneling-induced instabilities in the driven dissipative bose-hubbard model, *Phys. Rev. Lett.* **110**, 233601 (2013).
- [37] A. Le Boité, G. Orso, and C. Ciuti, Bose-hubbard model: Relation between driven-dissipative steady states and

- equilibrium quantum phases, *Phys. Rev. A* **90**, 063821 (2014).
- [38] R. M. Wilson, K. W. Mahmud, A. Hu, A. V. Gorshkov, M. Hafezi, and M. Foss-Feig, Collective phases of strongly interacting cavity photons, *Phys. Rev. A* **94**, 033801 (2016).
- [39] V. Savona, Spontaneous symmetry breaking in a quadratically driven nonlinear photonic lattice, *Phys. Rev. A* **96**, 033826 (2017).
- [40] M. Biondi, G. Blatter, H. E. Türeci, and S. Schmidt, Nonequilibrium gas-liquid transition in the driven-dissipative photonic lattice, *Phys. Rev. A* **96**, 043809 (2017).
- [41] M. Biondi, S. Lienhard, G. Blatter, H. E. Türeci, and S. Schmidt, Spatial correlations in driven-dissipative photonic lattices, *New Journal of Physics* **19**, 125016 (2017).
- [42] A. Tomadin, V. Giovannetti, R. Fazio, D. Gerace, I. Carusotto, H. E. Türeci, and A. Imamoglu, Signatures of the superfluid-insulator phase transition in laser-driven dissipative nonlinear cavity arrays, *Phys. Rev. A* **81**, 061801 (2010).
- [43] D. Huybrechts and M. Wouters, Dynamical hysteresis properties of the driven-dissipative bose-hubbard model with a gutzwiller monte carlo approach, *Phys. Rev. A* **102**, 053706 (2020).
- [44] P. Deuar, A. Ferrier, M. Matuszewski, G. Orso, and M. H. Szymańska, Fully quantum scalable description of driven-dissipative lattice models, *PRX Quantum* **2**, 010319 (2021).
- [45] S. Finazzi, A. Le Boité, F. Storme, A. Baksic, and C. Ciuti, Corner-space renormalization method for driven-dissipative two-dimensional correlated systems, *Phys. Rev. Lett.* **115**, 080604 (2015).
- [46] L. M. Sieberer, S. D. Huber, E. Altman, and S. Diehl, Dynamical critical phenomena in driven-dissipative systems, *Phys. Rev. Lett.* **110**, 195301 (2013).
- [47] F. Vicentini, F. Minganti, R. Rota, G. Orso, and C. Ciuti, Critical slowing down in driven-dissipative bose-hubbard lattices, *Phys. Rev. A* **97**, 013853 (2018).
- [48] J. J. Mendoza-Arenas, S. R. Clark, S. Felicetti, G. Romero, E. Solano, D. G. Angelakis, and D. Jaksch, Beyond mean-field bistability in driven-dissipative lattices: Bunching-antibunching transition and quantum simulation, *Phys. Rev. A* **93**, 023821 (2016).
- [49] D. Jaschke, S. Montangero, and L. D. Carr, One-dimensional many-body entangled open quantum systems with tensor network methods, *Quantum science and technology* **4**, 013001 (2018).
- [50] H. Weimer, A. Kshetrimayum, and R. Orús, Simulation methods for open quantum many-body systems, *Rev. Mod. Phys.* **93**, 015008 (2021).
- [51] W. Casteels, S. Finazzi, A. Le Boite, F. Storme, and C. Ciuti, Truncated correlation hierarchy schemes for driven-dissipative multimode quantum systems, *New Journal of Physics* **18**, 093007 (2016).
- [52] D. Roberts and A. A. Clerk, Competition between two-photon driving, dissipation, and interactions in bosonic lattice models: An exact solution, *Phys. Rev. Lett.* **130**, 063601 (2023).
- [53] D. Manzano, A short introduction to the lindblad master equation, *Aip advances* **10** (2020).
- [54] H.-P. Breuer and F. Petruccione, *The theory of open quantum systems* (Oxford University Press, USA, 2002).
- [55] R. Hanai, P. B. Littlewood, and Y. Ohashi, Photoluminescence and gain/absorption spectra of a driven-dissipative electron-hole-photon condensate, *Phys. Rev. B* **97**, 245302 (2018).
- [56] X. Wang, C. Xiao, H. Park, J. Zhu, C. Wang, T. Taniguchi, K. Watanabe, J. Yan, D. Xiao, D. R. Gamelin, *et al.*, Light-induced ferromagnetism in moiré superlattices, *Nature* **604**, 468 (2022).
- [57] P. Kirton, M. M. Roses, J. Keeling, and E. G. Dalla Torre, Introduction to the dicke model: From equilibrium to nonequilibrium, and vice versa, *Advanced Quantum Technologies* **2**, 1800043 (2019).
- [58] J. Cardy, *Finite-size scaling* (Elsevier, 2012).
- [59] Y. Zhang and T. Barthel, Criticality and phase classification for quadratic open quantum many-body systems, *Phys. Rev. Lett.* **129**, 120401 (2022).
- [60] S. Sachdev, *Quantum Phase Transitions*, 2nd ed. (Cambridge University Press, 2011).

Appendix A: Condition for diagonal steady state

Given a generic Hamiltonian $H = H_S + H_R + \sum_{\alpha} S_{\alpha} \otimes R_{\alpha}$, with S_{α} a system operator and R_{α} a reservoir operator, we can separate it into a system (H_S), reservoir (H_R), and interaction piece. The resulting master equation for the density matrix of the system has the form in the weak-coupling limit [54]

$$\dot{\rho}_S = -i[H_S + H_{LS}, \rho_S] + \sum_{\omega, \alpha, \beta} \gamma_{\alpha, \beta}(\omega) \mathcal{L}(S_{\beta}(\omega), S_{\alpha}^{\dagger}(\omega))[\rho] \quad (\text{A1})$$

where $S_{\alpha}(\omega) = \sum_{E' - E = \omega} \Pi(E) S_{\alpha} \Pi(E')$ with $\Pi(E)$ the projector on the energy E eigenspace of H_S , and $H_{LS} = \sum_E \Pi(E) H_{LS, E} \Pi(E)$ is the Lamb shift Hamiltonian. As before $\gamma_{\alpha, \beta}(\omega)$ is expressed as correlators of the $R_{\alpha, \beta}$.

We now will assume that the density matrix only has coherences within each eigensector and show that it remains in this form under time evolution. To do so, we write the density matrix as $\rho_S = \sum_E \Pi(E) \rho(E) \Pi(E)$ where $\rho(E)$ is density matrix acting on the energy E eigenspace. For this form, we can explicitly compute

$$\begin{aligned} \dot{\rho}_S &= -i[H_S + H_{LS}, \rho_S] + \mathcal{D}[\rho] \\ &= \sum_E \Pi(E) [H_{LS, E}, \rho(E)] \Pi(E) + \mathcal{D}[\rho] \end{aligned}$$

with dissipative part

$$\mathcal{D}[\rho] = \sum_{\omega, \alpha, \beta} \gamma_{\alpha, \beta}(\omega) \sum_{E' - E = \omega} \left(\Pi(E) S_{\beta} \Pi(E') \rho(E') \Pi(E') S_{\alpha}^{\dagger} \Pi(E) \right. \\ \left. - \frac{1}{2} \Pi(E') S_{\alpha}^{\dagger} \Pi(E) S_{\beta} \Pi(E') \rho(E') \Pi(E') - \frac{1}{2} \Pi(E') \rho(E') \Pi(E') S_{\alpha}^{\dagger} \Pi(E) S_{\beta} \Pi(E') \right) \quad (\text{A2})$$

We therefore see that the density matrix remains block diagonal in the different energy sectors. We can always search for a steady state of this form, especially since we can always start from a ground state. We then turn on incoherent pumping, which will never create coherences between different energy blocks. The only way to create and maintain such coherences in this limit would be through a time-dependent H_S .

An immediate consequence of this result is that if the spectrum of H_S is non-degenerate, then the steady-state density matrix will be diagonal, $\rho = \sum_E \rho_E |E\rangle\langle E|$. However, this condition is not necessary.

In our above analysis, we always have diagonal damping rates $\gamma_{\alpha, \beta}(\omega) = \gamma_{\alpha, \alpha}(\omega) = \gamma_{\alpha}(\omega)$ with $\gamma_+(\omega) = I(\omega)$ [$\gamma_-(\omega) = \gamma(\omega)$] for corresponding operator $S_+ = \mathcal{B}^{\dagger}$ ($S_- = \mathcal{B}$), respectively. To find a diagonal ρ in this case, we just need that in some basis of each eigensector, $S_{\pm}(\omega)|E, m\rangle \propto |E \pm \omega, k\rangle$ (where m, k are indexing the degeneracy), i.e. the choice of basis leads to jump operators that do not create coherences between states of the same energy. This condition ensures that a density matrix $\rho = \sum_{E, m} \rho_{E, m} |E, m\rangle\langle E, m|$ stays of this form. Notably, since there is a conserved quantity N_B in our model that is changed by the S_{\pm} , it is clear that this condition will always hold if there is no degeneracy within each fixed N_B sector. If there is such degeneracy, the density matrix will still have a diagonal form if $S_{\pm}(\omega)$ does not generate superpositions of degenerate states. Writing this condition in the notation of the main text gives the result as stated there.

Appendix B: Standard assumption of Lindblad operators

Let's analyze the case with $t = 0$ with the form of the jump operators from e.g. Refs [36, 37]. We have

$$H_0 = \mu \sum_i \left(n_i + \frac{U}{2} n_i (n_i - 1) \right) \\ \dot{\rho}(t) = -i[H_0, \rho] + \sum_i (\gamma \mathcal{L}(b_i, b_i^{\dagger})[\rho] + I \mathcal{L}(b_i^{\dagger}, b_i)[\rho]) \quad (\text{B1})$$

In this case, the sites are decoupled and $\rho = \bigotimes_i \rho_i$. We can therefore consider only one site at a time. We write out the density matrix in the number basis $\rho_i = \sum_{n=0}^M \rho_{i, n} |n_i\rangle\langle n_i|$, whose form is preserved under time evolution, and we find

$$\dot{\rho}_{i, n} = (n+1)(\gamma \rho_{i, n+1} - I \rho_{i, n}) + n(I \rho_{i, n-1} - \gamma \rho_{i, n}). \quad (\text{B2})$$

As in the main text, we see that the form $\rho_{i, n} = \rho_{i, 0} (I/\gamma)^n$ is a solution.

There are at least two shortcomings to this formalism, however, that are apparent even in this simple example: first, this steady state appears to not depend at all on the parameters of H_0 (as opposed to our solution where U/μ affects the location of the transitions). Second, it is not clear how to include temperature. If we assume that the bath has a temperature T , there is no clear way to include it in the definition of I and γ because they lack a dependence on the energy. One natural way would be to assume $I/\gamma = e^{-\mu/T}$, but the fact that the energy is quadratic in n means that the steady state cannot fit the thermal form $\rho_n = e^{-(\mu n + U n(n-1)/2)/T}$. As we discuss in the main text, our approach readily capture the coupling to a thermal reservoir, which leads to the steady-state density matrix being of the Boltzmann form $\rho \sim e^{-H/T}$, a well-known attribute of the weak-coupling limit Lindblad formalism [54].

Appendix C: Short-ranged or long-ranged Lindblad operators?

In our text, we assumed that the wavelength of light was much larger than the extent of the system and therefore we took a translation-invariant coupling to our sites. In most other work, e.g. [36, 37], the opposite limit is chosen. How do we know which limit is applicable and/or how do we extrapolate between them?

The derivation of the master equation provides the answer. Let's assume the environment is solely composed of photons and the system and environment couple in the natural way, as before [55]

$$H_I = \sum_{\mathbf{k}, \pm} g_{\mathbf{k}, \pm} a_{\mathbf{k}, \pm} b_{\mathbf{k}}^{\dagger} + \text{H.c.} = \sum_i \mathcal{R}_i b_i^{\dagger} + \text{H.c.} \quad (\text{C1})$$

where $\mathcal{R}_i = \frac{1}{\sqrt{N}} \sum_{\mathbf{k}, \pm} g_{\mathbf{k}, \pm} a_{\mathbf{k}, \pm} e^{i\mathbf{x}_i \cdot \mathbf{k}}$.

Regardless of what the system Hamiltonian is (assuming it satisfies the assumptions needed for the derivation of the master equation), the environment will only enter through the computation of

$$\gamma_{i, j}(\omega) = \int_{-\infty}^{\infty} ds e^{i\omega s} \langle \mathcal{R}_i(s) \mathcal{R}_j^{\dagger} \rangle; \\ I_{i, j}(\omega) = \int_{-\infty}^{\infty} ds e^{i\omega s} \langle \mathcal{R}_i^{\dagger}(s) \mathcal{R}_j \rangle$$

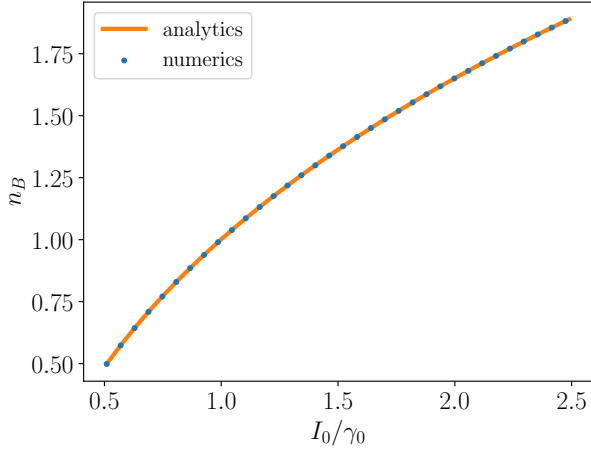


Figure S.1. The analytical and numerical results for $U = 0$.

The computation is almost identical, so we just focus on

$$\gamma_{i,j}(\omega) = \frac{1}{N} \sum_{\mathbf{k}, \pm} 2\pi\delta(\omega - k) |g_{\mathbf{k}, \pm}|^2 e^{i(\mathbf{x}_i - \mathbf{x}_j) \cdot \mathbf{k}} n_{\mathbf{k}} \quad (\text{C2})$$

where we assumed that $H_R = \sum_{\mathbf{k}, \pm} k a_{\mathbf{k}, \pm}^\dagger a_{\mathbf{k}, \pm}$ and a thermal distribution of light with $\langle a_{\mathbf{k}, \pm}^\dagger a_{\mathbf{k}, \pm} \rangle = n_{\mathbf{k}}$. In order to evaluate further, we need to know what the $g_{\mathbf{k}, \pm}$ are, which depend on the details of the system. Here we just assume it varies smoothly with \mathbf{k} . We note that, when $|\mathbf{x}_i - \mathbf{x}_j|k \gg 1$, with k set by ω , the angular integral will lead to terms that average to zero for $i \neq j$, and thus the dissipative part takes the form $\sum_i \gamma \mathcal{L}(L_i, L_i^\dagger)$, i.e. local pump and decay apply here. However, when $|\mathbf{x}_i - \mathbf{x}_j|k \ll 1$, it is clear that the jump operators arising from \mathcal{R}_i and \mathcal{R}_j will mix together, and then we have a dissipative term of the form $\gamma \mathcal{L}(\sum_i L_i, \sum_j L_j^\dagger)$. In the latter case, we just recover the situation considered in the main text, i.e. a global pump and decay.

Appendix D: Analytic solution of $U/t = 0$ limit

As we stated in the text, the full eigensystem information of H_S can be hard to obtain, but only the eigenstates that are connected by the derived Lindblad operators are relevant. Here we demonstrate this idea in the $U/t = 0$ limit of the Bose Hubbard model, where we can also obtain an analytical solution of the steady state. In this case, it's better to reformulate the system Hamiltonian as a spin- $M/2$ system, so that we can have a direct comparison with the numerics which imposes a boson number truncation M . To do so, we just need to redefine the action of b_i in H_0 by

$$\begin{aligned} b_i |n_i\rangle &= \sqrt{n_i(M+1-n_i)} |(n-1)_i\rangle; \\ b_i^\dagger |n_i\rangle &= \sqrt{(n+1)(M-n)} |(n+1)_i\rangle; \\ \hat{n}_i |n_i\rangle &= n_i |n_i\rangle. \end{aligned}$$

These map to spin- $M/2$ operators $b_i^\dagger \rightarrow S_i^+$, $b_i \rightarrow S_i^-$, and $\hat{n}_i \rightarrow S_i^z + M/2$ satisfying the usual commutation relations. We then have the system Hamiltonian

$$H_s = \mu \sum_i \hat{n}_i - \frac{t}{N} \sum_{i,j} b_i^\dagger b_j \quad (\text{D1})$$

We still define the coupling operator $\mathcal{B} = \sum_i b_i$. One can then verify the commutation relation:

$$[H_s, \mathcal{B}] = (-\mu + Mt - \frac{2t}{N} \hat{N}_B) \mathcal{B}. \quad (\text{D2})$$

Note that \mathcal{B} is not an eigenoperator since \hat{N}_B is an operator. But we can decompose \mathcal{B} as

$$\mathcal{B} = \sum_{N_B} \mathcal{B}_{N_B} \quad (\text{D3})$$

where $\mathcal{B}_{N_B} \equiv P_{N_B-1} \mathcal{B} P_{N_B}$, and P_{N_B} is the projector onto the sector of boson number N_B . Then, one can verify

$$[H_s, \mathcal{B}_{N_B}] = (-\mu + Mt - 2t \frac{N_B - 1}{N}) \mathcal{B}_{N_B} \quad (\text{D4})$$

and thus \mathcal{B}_{N_B} are eigenoperators, with energies $\omega_{N_B} = \mu - t(M - \frac{2(N_B-1)}{N})$, which have the same form as in the $M = 1(U/t \neq 0)$ case in the text. In the $M = 1(U/t \neq 0)$ case, each N_B sector has only one eigenstate and thus we can label them by $|N_B\rangle$ and write down the master equation in such basis. Here in each N_B sector, there are clearly more than one eigenstate. However, since we start from the vacuum state, all the states visited during the Lindblad time evolution are those generated by the Lindblad operators, i.e. we may still denote $|N_B\rangle \equiv C_{N_B}(\mathcal{B})^{N_B} |\text{vac}\rangle$, with C_{N_B} being the normalization factor. One can check that $\mathcal{B}(\mathcal{B}^\dagger)$ acting on the normalized $|N_B\rangle$ gives us $\sqrt{N_B(NM - 2N_B)} |N_B - 1\rangle (\sqrt{(N_B + 1)(NM - 2N_B)} |N_B + 1\rangle)$. Then, we can write down the master equation accordingly, and the solution would have the same structure as in $M = 1(U/t \neq 0)$.

We compare the analytical solution with the numerics in Fig. S.1. The alignment between them confirms our arguments above.

Appendix E: Derivation of $M = 1$ density matrices and observables

We first consider the Mott phase, where $r_< = I(\mu - t)/\gamma(\mu - t) \ll 1$ or $r_> = I(\mu + t)/\gamma(\mu + t) \gg 1$. For $r_< < 1$, from Eq. (26) in the main text, we have

$$\begin{aligned}
\rho_m &= \rho_0 \prod_{j=1}^m r(\omega_j) \\
&= \rho_0 r_{<}^m \prod_{j=1}^m \left(1 + \frac{r'_{<} 2tj}{r_{<} N}\right) \\
&\approx \rho_0 r_{<}^m \exp\left(\sum_{j=1}^m \frac{2r'_{<} t}{r_{<} N} j\right) \\
&\approx \rho_0 r_{<}^m \exp\left(\frac{r'_{<} t}{r_{<} N} m^2\right)
\end{aligned}$$

where we Taylor expand r_j , convert the product to the exponential of a sum, and keep only the leading order term in a $1/N$ expansion of the exponential. The weight ρ_m/ρ_0 at large m is suppressed by $r_{<}^m$ as well as the exponential function. This calculation is controlled because $m \lesssim \sqrt{N}$ are the only values where ρ_m is substantial (if $r_{<} \leq 1$).

When $r_{<} \ll 1$, ρ_m decays very fast and we are in the deep Mott phase. Note that $r'_{<} < 0$ is exactly our assumption that $r(\omega)$ monotonically decreases, as stated in the text. Similarly, we can consider the case $r_{>} \gg 1$, and we get

$$\rho_{N-m} = \rho_N \prod_{j=0}^{m-1} [r(\omega_{N-j})]^{-1} \approx \rho_N r_{>}^{-m} \exp\left(\frac{r'_{>} t}{N} m^2\right) \quad (\text{E1})$$

Next, we analyze the intermediate phase, when $r_{<} > 1 > r_{>}$ and $r_{j^*} = 1$ with $j^*/N \sim O(1)$. An almost identical calculation gives

$$\begin{aligned}
\rho_{j^*+m} &= \begin{cases} \rho_{j^*} \prod_{j=0}^m \left(1 + r'_{j^*} \frac{2tj}{N}\right) & m \geq 0 \\ \rho_{j^*} \prod_{j=0}^{-m} \left(1 - r'_{j^*} \frac{2tj}{N}\right)^{-1} & m \leq 0 \end{cases} \\
&\approx \rho_{j^*} \exp\left(\frac{r'_{j^*} t}{N} m^2\right)
\end{aligned}$$

where we used $r_{j^*} = 1$, and thus we have only an exponential decay term compared to the Mott phase, which would be slower since the exponent is suppressed by $1/N$. This holds true until m^2 reaches N , where the density matrix weight is already negligible. Therefore, we should have $m \lesssim \sqrt{N}$. For j^* near 0 or N , $j^* \pm m$ should be truncated by 0 and N , respectively.

Now, we can calculate the observables and critical behaviors. Deep inside the superfluid phase, we have the order parameter $\Psi^2 = \langle \mathcal{B}^\dagger \mathcal{B} \rangle / N^2$

$$\begin{aligned}
\Psi^2 &= \frac{\sum_m (j^* + m)(N - j^* - m + 1) \exp\left(\frac{r'_{j^*} t}{N} m^2\right)}{N^2 \left(\sum_m \exp\left(\frac{r'_{j^*} t}{N} m^2\right)\right)} \\
&\approx \frac{j^*}{N} \left(1 - \frac{j^*}{N}\right) + O(1/\sqrt{N}) \quad (\text{E2})
\end{aligned}$$

where m is summed from $-j^*$ to $N - j^*$ but only the terms with $|m| \lesssim \sqrt{N}$ contribute. We keep only the leading order terms.

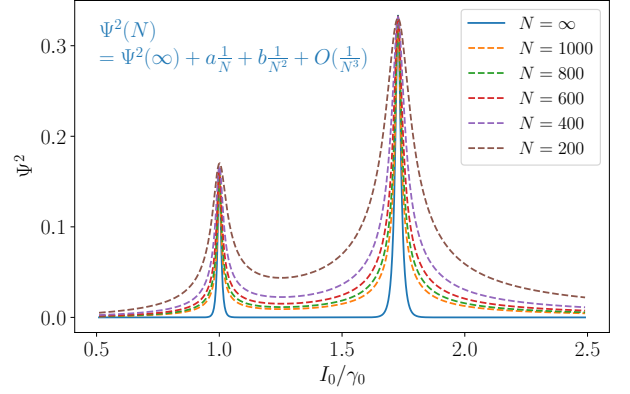


Figure S.2. The details of extrapolation to $N = \infty$ for Ψ^2 for $M = 2$ at $t = 0, U = 30, \mu = 150$. The same procedures are carried out for other t/U values and other observables.

From the Mott phase side, we can calculate Ψ^2 as well. We assume $r_{<} \ll 1$, we can ignore the exponential corrections and evaluate

$$\begin{aligned}
\Psi^2 &= \frac{\sum_{m=0}^N m(N - m + 1) r_{<}^m \exp\left(\frac{r'_{<} t}{N} m^2\right)}{N^2 \left(\sum_{m=0}^N r_{<}^m \exp\left(\frac{r'_{<} t}{N} m^2\right)\right)} \\
&\approx \frac{1}{N} \left(\frac{\sum_m m r_{<}^m}{\sum_m r_{<}^m}\right) \\
&= \frac{1}{N} \frac{r_{<}}{1 - r_{<}}
\end{aligned}$$

A similar calculation for $r_{>} \gg 1$ holds and we find $\Psi^2 \approx (1 - r_{>}^{-1})^{-1}/N$.

Finally, if we approach the phase transition from the left, $r_{<} \rightarrow 1^-$, we use $r_{<}^m = e^{\ln(r_{<}^m)} \approx e^{m(r_{<} - 1)}$ to write

$$\begin{aligned}
\Psi^2 &\approx \frac{1}{N^2} \frac{\rho_0 \sum_{m=0}^N m(N - m + 1) e^{\frac{r'_{<} t}{N} m^2 + m(r_{<} - 1)}}{\rho_0 \sum_{m=0}^N e^{\frac{r'_{<} t}{N} m^2 + m(r_{<} - 1)}} \\
&\approx \frac{1}{N^{1/2}} \frac{\int_0^{\sqrt{N}} dx x \exp\left[\frac{r'_{<} t}{N} x^2 - (1 - r_{<}) \sqrt{N} x\right]}{\int_0^{\sqrt{N}} dx \exp\left[\frac{r'_{<} t}{N} x^2 - (1 - r_{<}) \sqrt{N} x\right]}.
\end{aligned}$$

where we changed to the variable $x = m/\sqrt{N}$ and approximated the sums by integrals. The integrand quickly decays when $x \gtrsim 1$ so we can extend the limits of integration to infinity, and we then get the scaling form $\Psi^2 = N^{-1/2} f_s(N^{1/2}(1 - r_{<}))$. We verified that the same scaling form applies when we approach the phase transition from either side, and $n_B = \langle N_B \rangle / N$ has a scaling form with the same critical exponents as well.

Appendix F: Extrapolation details

In our numerical calculations, the lattice size can be up to 1000 for $M = 2$ and 100 for $M = 3$, within our computational capability. To get the phase diagram shown

in the text, we extrapolate the data at each point of t/U and I_0/γ_0 of several system sizes to thermodynamic limit ($N = \infty$). We use a polynomial extrapolation of order 2 (quadratic fitting), which is equivalent to assuming $O(N) = O(N = \infty) + O' \frac{1}{N} + O'' \frac{1}{N^2} + \dots$ and truncate it up to the second order of $1/N$. We find that the truncation up to quadratic order already gives us fair results. The fitting detail is shown in Fig. S.2, where not all finite N curves are plotted. For the extrapolation of the entropy, we get negative extrapolated entropy values at negligibly few points. We manually set them to be 0 since a negative entropy is not physical and we believe this abnormal behavior is a numerical artifact during the extrapolation. We also tried a power law fitting in $1/N$, which gives almost the same results but fails near the phase transitions. We adopt the polynomial fitting results for it gives a more smooth behavior globally.

Appendix G: Phase diagrams

In the text we showed the phase diagram in terms of Ψ^2 . Here we show the phase diagrams mapped in terms of n_B and S/N in Fig. S.3. We see that the extracted phase boundaries from the entropy clearly delineate the Mott regions seen in the n_B plot.

We also show the phase diagram for $M = 3$, by plotting Ψ^2 and n_B vs. I_0/γ_0 and $t/(t + U)$ in Fig. S.4. In this case, we can only reach up to $N = 70$, but we can already see the Mott insulating domes appearing. The shape of the $n_B = 2$ lobe is clearly very different from the $M = 2$ case, but the $n_B = 1$ lobe appears very similar. This plot demonstrates that the effect of the truncation is unlikely to affect the physics near the $n_B = 1$ lobe.

Appendix H: Critical scaling

1. Mott-Mott transition

In the main text, we studied n_B , the order parameter for characterizing the Mott-Mott transition point, and confirmed the critical scaling form $n_B = f_{n_B, m}(N(I_0 - I_c))$. In Fig. S.5 we show the scaling collapse for Ψ^2 at this transition point, and the same scaling form as n_B also applies here i.e. $\Psi^2 = f_{\Psi^2, m}(N(I_0 - I_c))$.

2. Mott-Superfluid transition

In the main text, we displayed the critical scaling from Mott to superfluid phases by tuning $r = I_0/\gamma_0$, where we confirmed the scaling form $\Psi^2(N) = N^{-1/2} f_{\Psi^2, s}(\sqrt{N}(r - r_c))$. In Fig. S.6 we show that this scaling form applies if we tune t/U at fixed I_0/γ_0 instead, and, in both cases, the same exponents are found.

We expect that this scaling form should almost everywhere at the Mott-superfluid phase boundary. In

the equilibrium case, there are two different universality classes for the Mott-superfluid transition depending on whether the density remains at $n_B \in \mathbb{Z}$ (at the peak of the Mott lobe) or if the density is generic [60]. The two can be distinguished as having different values of the dynamic critical exponent, z . In principle, the Liouvillian gap, described in the next section, determines how quickly the system approaches the steady state and could probe z . In practice, we can only reach the scaling regime for the Liouvillian gap for $M = 1$, which does not have the ‘‘special’’ critical point as there is no peak of the Mott lobe.

3. Liouvillian gap

The Liouvillian, \mathcal{L} , is the superoperator defining the right-hand-side of the master equation $\dot{\rho} = \mathcal{L}\rho$. Here we measure the Liouvillian gap, $\Delta_{\mathcal{L}}$ defined as the smallest real part of the non-zero eigenvalues of \mathcal{L} [59]. This gap determines the characteristic time for the system to reach its steady state. In Fig. S.7, it’s clear that $\Delta_{\mathcal{L}}$ reaches a minimum at the (Mott-superfluid) phase boundary, which implies a critical slowing down near the phase transitions. As in the superradiance phenomenon, the system decay rate scales with N [54], so we rescaled $\Delta_{\mathcal{L}}/N$ to make it clear that there is a slowing down at the phase transition relative to the rest of the phase diagram.

In Fig. S.8, we perform a scaling collapse for $\Delta_{\mathcal{L}}$ with $M = 1$. In equilibrium, the energy gap $\Delta E \sim (t - t_c)^\delta$ where $\delta = \nu z$ for z the dynamic critical exponent and ν the correlation length exponent. In the mean-field theory of the equilibrium Bose-Hubbard model $\delta = 1$. Similarly, we see that $\Delta_{\mathcal{L}}/N = N^{-\delta'/\lambda} g_{\mathcal{L}}(N^{1/\lambda}(I_0 - I_c))$ for some scaling function $g_{\mathcal{L}}$ and exponent δ', λ (that are potentially different between the Mott-Mott and Mott-superfluid transition) implying that $\Delta_{\mathcal{L}}/N \sim (I_0 - I_c)^{\delta'}$ close to the transition. We numerically observe $\delta'_s = \delta'_m = 1$ (as well as $\lambda_m = \lambda_s - 1 = 1$ as before) similar to $\delta_s = 1$ for the equilibrium transition. We consider $\Delta_{\mathcal{L}}/N$ instead of $\Delta_{\mathcal{L}}$ so that a finite value is reached away from the critical point in the thermodynamic limit.

Calculations of $\Delta_{\mathcal{L}}$ for $M \geq 2$ are beyond our computational capabilities, but we expect that the slowing-down and scaling form do not depend on the truncation M and will hold for general M .

Appendix I: Steady state distributions

It’s worth noting that in our model, the resulting steady states are non-thermal. In Fig. S.9, we display the steady state density matrix distribution with respect to system energy obtained by numerics at a generic point in the phase space ($I_0/\gamma_0 = 1.26, t/(t + U) = 0.1$), and $M = 2$. In the inset, we can see a oscillation feature within each N_B sector, which emphasizes the non-thermal property of the steady state. The peak structure

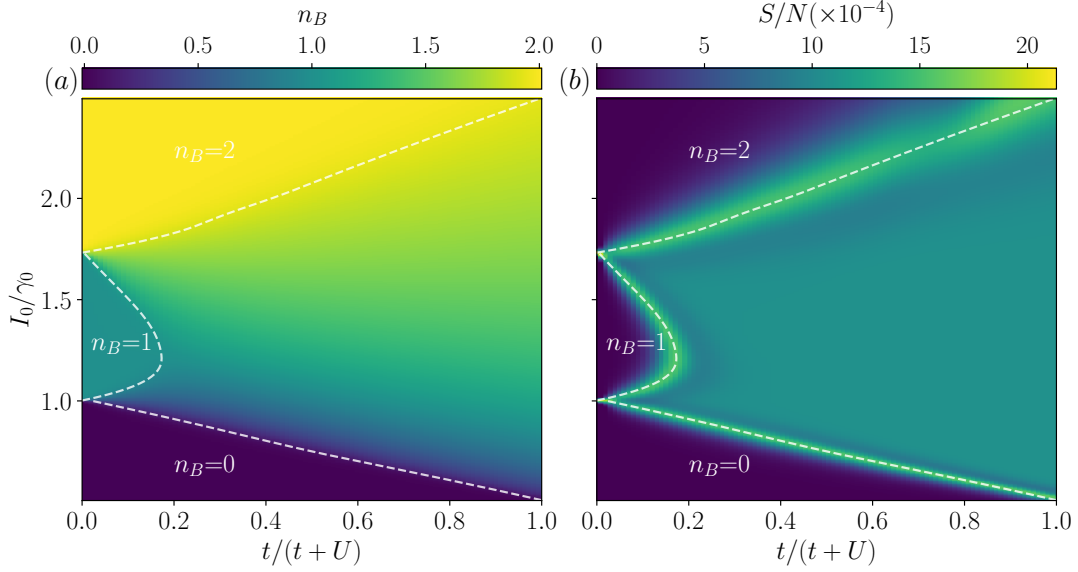


Figure S.3. The phase diagrams mapped in terms of (a) n_B and (b) S/N , for $M = 2$. Every data point is extrapolated to $N = \infty$ as indicated in the Supporting text.

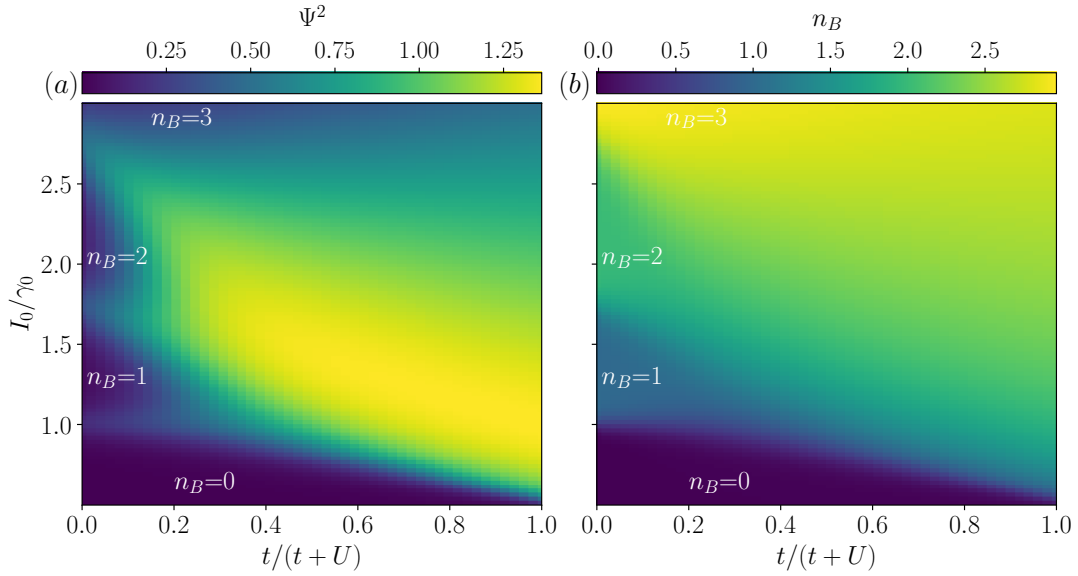


Figure S.4. The phase diagrams mapped in terms of (a) Ψ^2 and (b) n_B , for $M = 3$. We see the Mott lobes appearing; although the $n_B = 2$ region has now become a lobe, the $n_B = 1$ lobe seems almost identical.

of $\rho(E)$ cannot be explained through a grand canonical form for $\rho(E) \sim e^{-\beta(E-\mu N)}$.

Appendix J: Comparison with equilibrium system

In Fig. S.10, we show the (zero-temperature) equilibrium phase diagram of the all-to-all hopping Bose Hubbard Hamiltonian, in terms of $t/(t+U)$ and $\mu/(t+U)$, where μ is the bosonic chemical potential. The nonequilibrium and equilibrium phase diagrams have similar

shapes, which agrees with our intuition that increasing the intensity of the light is analogous to changing the chemical potential.

However, there are key differences: First, at $t/(t+U) = 0$, the order parameter Ψ^2 remains zero at any μ . This is different than the non-equilibrium case, where Ψ^2 has a peak and shows critical scaling at the transition point of two Mott lobes. Second, at any point in the phase diagram, the observables ($\Psi^2 = \langle \mathcal{B}^\dagger \mathcal{B} \rangle / N^2$ and $n_B = \langle N_B \rangle / N$) do not scale with N when N is large enough, which is reasonable since the all-to-all hopping

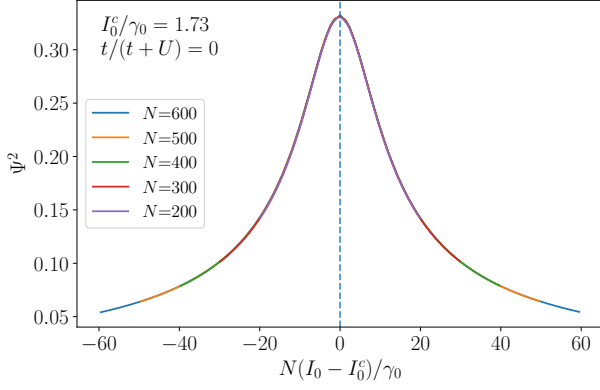


Figure S.5. Scaling collapses for Ψ^2 at the Mott-Mott transition.

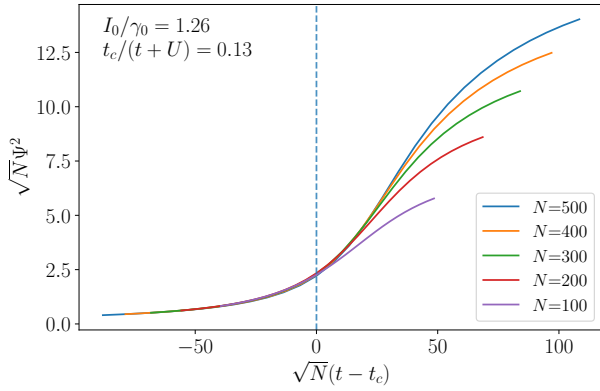


Figure S.6. Scaling collapses at the Mott-superfluid transition, where t/U is tuned and I_0/γ_0 is fixed.

is equivalent to enforcing a mean field behavior. Third, the entropy remains zero in the whole phase diagram, because at zero temperature, we are always at the ground state, which in general has no degeneracy. However, we observe a peak of entropy at the non-equilibrium phase transition.

Finally, we comment on the critical exponents. For the equilibrium Mott-Mott transition, we can only tune μ to move directly from e.g. the $n_B = 0$ to the $n_B = 1$ lobe. The transition is simply between the eigenstate with every site having 0 bosons and the eigenstate with every site having 1 bosons. By analyzing the energy per site, it is clear that this transition is first-order. In the nonequilibrium case, we find that this transition has become second order with an order parameter, e.g. $n_B = \Theta(I_0 - I_c)$ for the $n_B = 0$ to $n_B = 1$ lobe, that has the finite-size scaling form $n_B = N^{-\beta_m/\lambda_m} f_{n_B,m}(N^{1/\lambda_m}(I_0 - I_c))$ with $\lambda_m = \beta_m + 1 = 1$.

For the Mott-superfluid transition, as we mentioned above, there is a “generic” transition, occurring in most of the phase diagram, and a “special” transition occurring at the peak of the Mott lobe. Both critical points have an energy gap that scales as $\Delta E \sim (t - t_c)^{\nu z}$ with $\nu z = 1$ but the former has $z = 2$ and the latter $z = 1$. We are unsure if we can capture the “special” transition in our nonequilibrium model, but we can determine the critical exponents β_s and λ_s as before for the generic case.

Our all-to-all model mimics the mean-field limit of the Bose-Hubbard model [1], and we can then immediately know that the mean-field value of $\beta_s = 1$ (since our order parameter is Ψ^2 and not Ψ). In fact, we can predict the scaling behaviors through a path integral formulation. The partition function, with an applied external field $(-h^*b_i - hb_i^\dagger)$, is given by

$$Z(h) = \int \mathcal{D}b_i \mathcal{D}b_i^* e^{-\int d\tau \left(-\frac{t}{N} (\sum_i b_i^*) (\sum_j b_j) + \sum_i (b_i^* \partial_\tau b_i + U n_i^2 - \mu n_i) - \sum_i (h^* b_i + h b_i^*) \right)} \quad (\text{J1})$$

$$= \int \mathcal{D}b_i \mathcal{D}b_i^* \mathcal{D}\psi \mathcal{D}\psi^* e^{-\int d\tau \left(\sum_i \left((\psi^* - h^*) b_i + (\psi - h) b_i^* + b_i^* \partial_\tau b_i + U n_i^2 - \mu n_i \right) + \frac{N}{t} |\psi|^2 \right)} \quad (\text{J2})$$

In the second line, we make a Hubbard-Stratonovich transformation to decouple the hopping term, and only a single auxiliary field is needed due to the all-to-all hop-

ping form. Since all sites are decoupled, we can integrate out each b_i and arrive at an effective action for field ψ , where each b_i integration gives the same contribution.

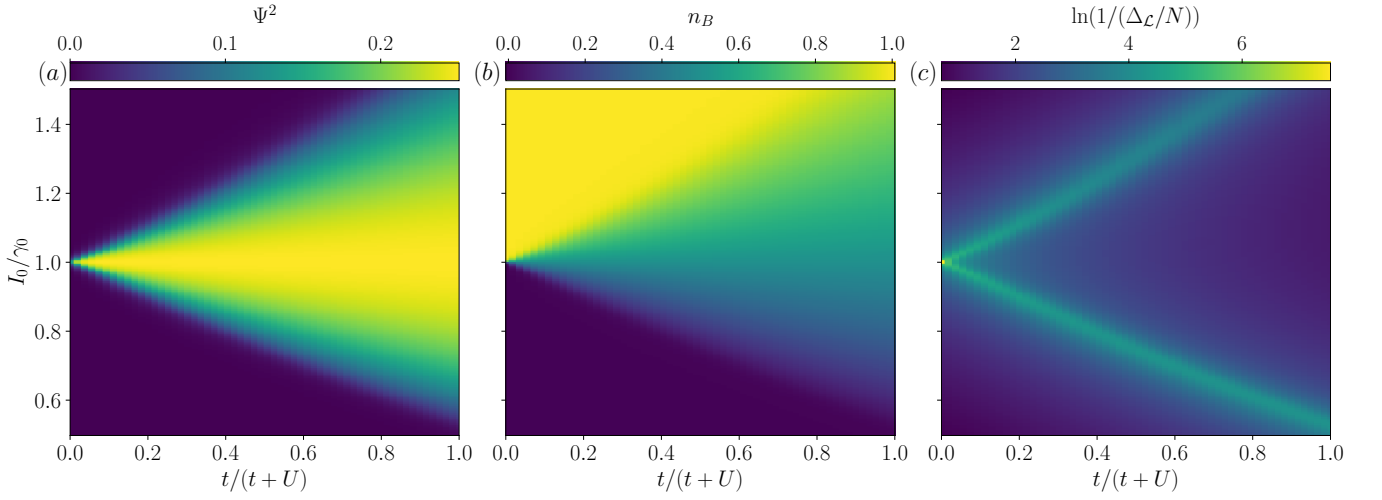


Figure S.7. We plot (a) Ψ^2 , (b) n_B and (c) the inverse Liouvillian gap on a log scale, for $M = 1$. We see that the Liouvillian gap is smallest at phase boundaries.

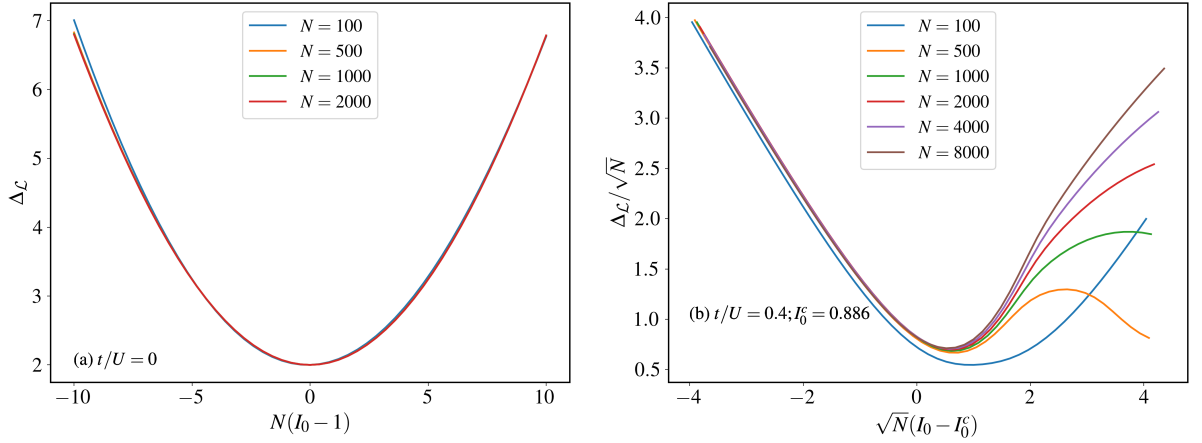


Figure S.8. We plot the Liouvillian gap scaling for the Mott-Mott (a) and Mott-superfluid (b) phase transitions for the $M = 1$ case. In both cases $\Delta_{\mathcal{L}} \sim N$ away from the critical point as in the superradiance case. The scaling collapse for the Mott-superfluid case has more finite-size effects due to the superfluid phase being an intermediate phase between two Mott phases.

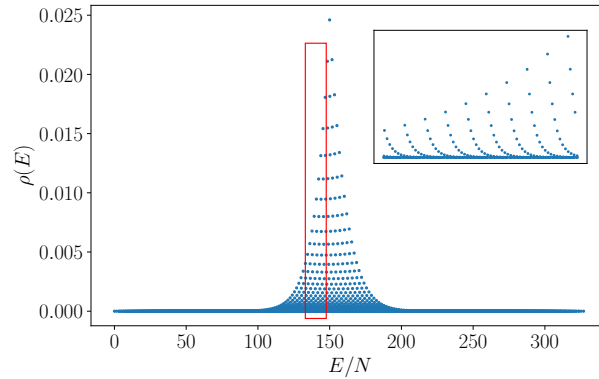


Figure S.9. The non-equilibrium steady state density matrix distribution for $M = 2$, at $I_0/\gamma_0 = 1.26$, $t/(t+U) = 0.1$. The inset is the zoomed-in region in the red rectangle.

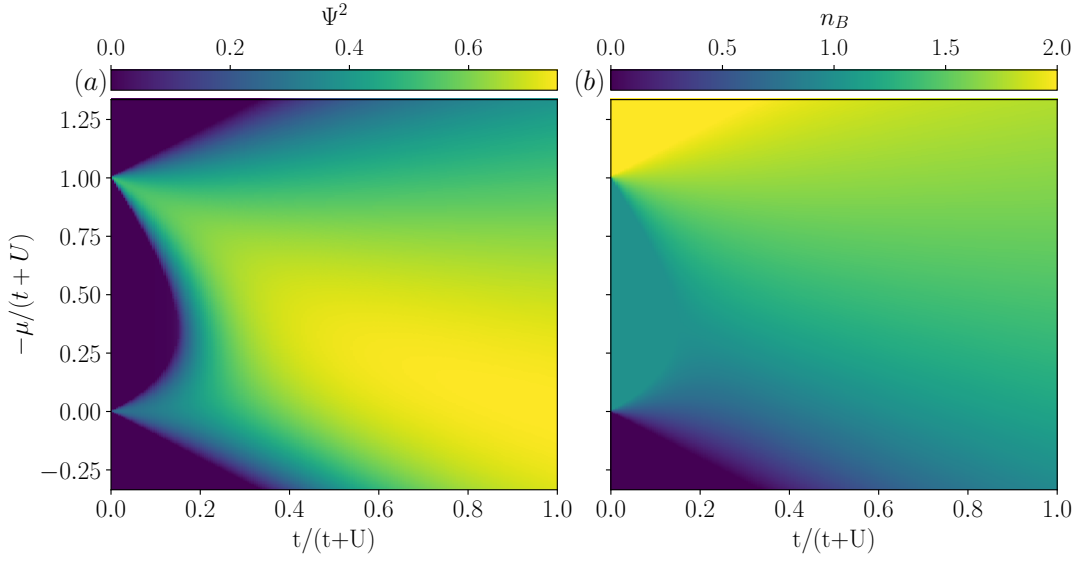


Figure S.10. The (zero-temperature) equilibrium phase diagrams for the all-to-all hopping Bose Hubbard model. The scaled observables Ψ^2 and n_B do not depend on N .

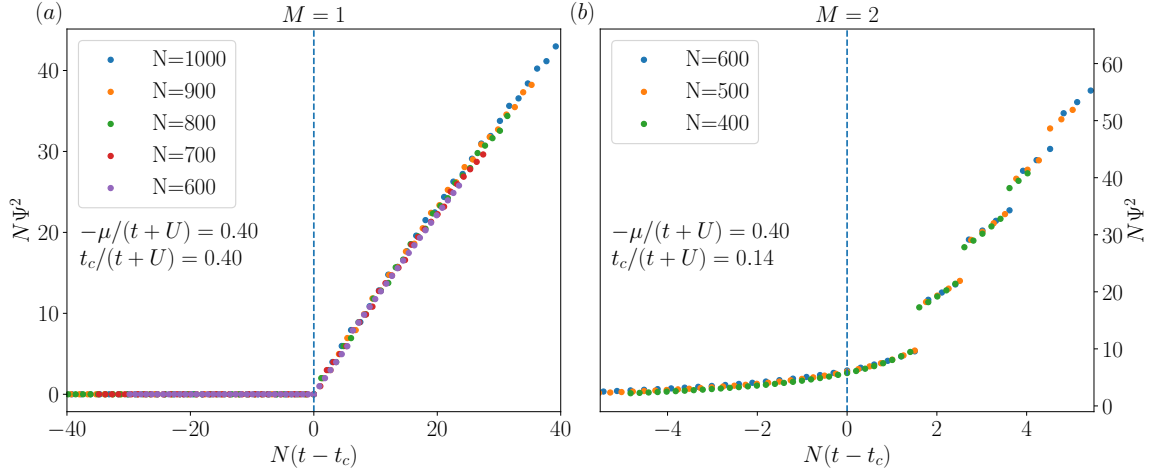


Figure S.11. We plot the scaling collapse for Ψ^2 for (a) $M = 1$ and (b) $M = 2$ respectively, for the transition from the Mott phase ($n_B = 1$) to the superfluid phase. We see that the equilibrium transition has $\lambda_s = 1$ as opposed to the nonequilibrium transition with $\lambda_s = 2$.

$$S_{\text{eff}} = \int d\tau \left(N f(\psi - h) - \frac{N}{t} |\psi^2| \right) \quad (\text{J3})$$

$$= \int d\tau N \left(r_0 |\psi - h|^2 + u_0 |\psi - h|^4 - \frac{1}{t} |\psi^2| + \dots \right) \quad (\text{J4})$$

$$= \int d\tau N \left(r_0 (|\psi|^2 - h^* \psi - h \psi^*) + u_0 (|\psi|^4 - 2h^* \psi |\psi|^2 + \text{c.c.}) - \frac{1}{t} |\psi^2| + \dots \right) \quad (\text{J5})$$

$$= \int d\tau N \left(r |\psi|^2 + u_0 |\psi|^4 - r_0 h \psi^* - 2u_0 h \psi^* |\psi|^2 + \text{c.c.} + \dots \right) \quad (\text{J6})$$

where $f(x)$ is some function obtained by integrating out b_i field. In the second line we Taylor expand $f(x)$ accord-

ing to symmetry constraints, and we ignored the Berry phase term $\psi^* \partial_\tau \psi$ as we assume that time-independent fields are most important at the saddle point [1]. In the third line we expand $|\psi - h|$ and omit terms of higher orders in h or eventually $1/N$. We define $r \equiv r_0 - 1/t$, and

$$S_{\text{eff}} = \int d\tau \left(|\psi|^2 + \frac{u_0}{N r^2} |\psi|^4 - \frac{r_0 \sqrt{N}}{\sqrt{r}} h \psi^* - \frac{2u_0}{\sqrt{N r^3}} h \psi^* |\psi|^2 + \text{c.c.} + \dots \right) \quad (\text{J7})$$

$$\sim \int d\tau \left(|\psi|^2 + \frac{u_0}{N \delta t^2} |\psi|^4 - \frac{r_0 \sqrt{N}}{\sqrt{\delta t}} h \psi^* - \frac{2u_0}{\sqrt{N \delta t^3}} h \psi^* |\psi|^2 + \text{c.c.} + \dots \right) \quad (\text{J8})$$

So, the free energy $f = -\frac{1}{\beta N} \ln Z = -\frac{1}{\beta N} \int \mathcal{D}\psi \mathcal{D}\psi^* e^{-S_{\text{eff}}}$ should take the form of

$$Nf(N, h) = F(N\delta t^2, h\sqrt{\frac{N}{\delta t}}, \frac{h}{\sqrt{N\delta t^3}}) \quad (\text{J9})$$

And we can calculate the order parameter Ψ^2 at zero external field as

$$\Psi^2 = \langle (\sum_i b_i^\dagger) (\sum_j b_j) \rangle / N^2 \quad (\text{J10})$$

$$= \frac{1}{N^2} \frac{\partial^2}{\partial h \partial h^*} F(N\delta t^2, h\sqrt{\frac{N}{\delta t}}, \frac{h}{\sqrt{N\delta t^3}}) \Big|_{h=0} \quad (\text{J11})$$

$$= \frac{G_1(N\delta t^2)}{N\delta t} + \frac{G_2(N\delta t^2)}{(N\delta t)^2} + \frac{G_3(N\delta t^2)}{(N\delta t)^3} \quad (\text{J12})$$

where $G_1(x)$, $G_2(x)$ and $G_3(x)$ are different unknown functions. When we perform finite-size scaling collapses, we fix the lattice size N , and examine $\Psi^2(N)$ near the critical point, i.e. $\delta t \sim 0$. Therefore, we should look at Ψ^2 at the limit $\delta t \rightarrow 0$.

Because $\Psi^2 \rightarrow 0$ at the transition, we must have $G_1(0) = G_2(0) = G_3(0) = 0$. If we assume that $G_i(x)$ can be Taylor expanded at $N\delta t^2 = 0$, we find $G'_3(0) = 0$ and $\Psi^2 = G'_1(0)\delta t + \frac{1}{N}G'_2(0) + \dots$. Equivalently, $N\Psi^2 \sim G'_1(0)N\delta t + G'_2(0) + \dots$, which is consistent with the scaling collapse we find numerically in Fig. S.11 for $M = 1$ and $M = 2$. We thus confirm that $\lambda_s = \beta_s = 1$

at the critical t_c , r should go to zero, and $r \sim \delta t = t - t_c$ to the lowest order. Now, we rescale $\psi \rightarrow \psi/\sqrt{Nr}$. If there is any change in the measure of $\int \mathcal{D}\psi$, it only contributes a constant term $C(N)$ to the free energy. Then, we have

at the ‘‘generic’’ transition point in the equilibrium case, in contrast to the nonequilibrium $\lambda_s = \beta_s + 1 = 2$.

As a double check, we can calculate the scaling forms in the case of $M = 1$ where an exact solution can be obtained. Recall that there is only one state in the (fully symmetrized) sector of N_B bosons, labeled as $|N_B\rangle$. We have

$$E_{N_B} = \mu N_B - \frac{t}{N} N_B (N - N_B + 1);$$

$$\frac{\mathcal{B}^\dagger \mathcal{B}}{N^2} |N_B\rangle = \frac{N_B}{N} \left(1 - \frac{N_B}{N} + \frac{1}{N} \right).$$

By treating $n_B = N_B/N$ as a continuous variable, it is easy to find that the Mott-superfluid transition occurs at $t_c = -\mu/(1 - \frac{1}{N}) \sim -\mu$, where we choose $\mu < 0$ to study the $n_B = 1$ to superfluid phase transition. For the $\mu > 0$ transition, the same analysis can be carried out. The order parameter can be obtained as

$$\Psi^2 = \begin{cases} \frac{1}{N} & t < t_c \\ \frac{1}{4} - \frac{\mu^2}{4t^2} + \frac{1}{2N} + \frac{1}{4N^2} & t > t_c \end{cases} \quad (\text{J13})$$

And we can expand $t = \delta t - \mu$ near the critical point. After keeping only the lowest order terms of δt (suitable for doing finite size scaling), we get

$$\Psi^2 \sim -\frac{\delta t}{2\mu} + \frac{1}{2N} + \frac{1}{4N^2} \quad (\text{J14})$$

This result confirms again that $\lambda_s = \beta_s = 1$, consistent with the result of path integral calculation and our numerical results (Fig. S.11).